Oceanography thesis

An investigation of the Faroe Shelf Front

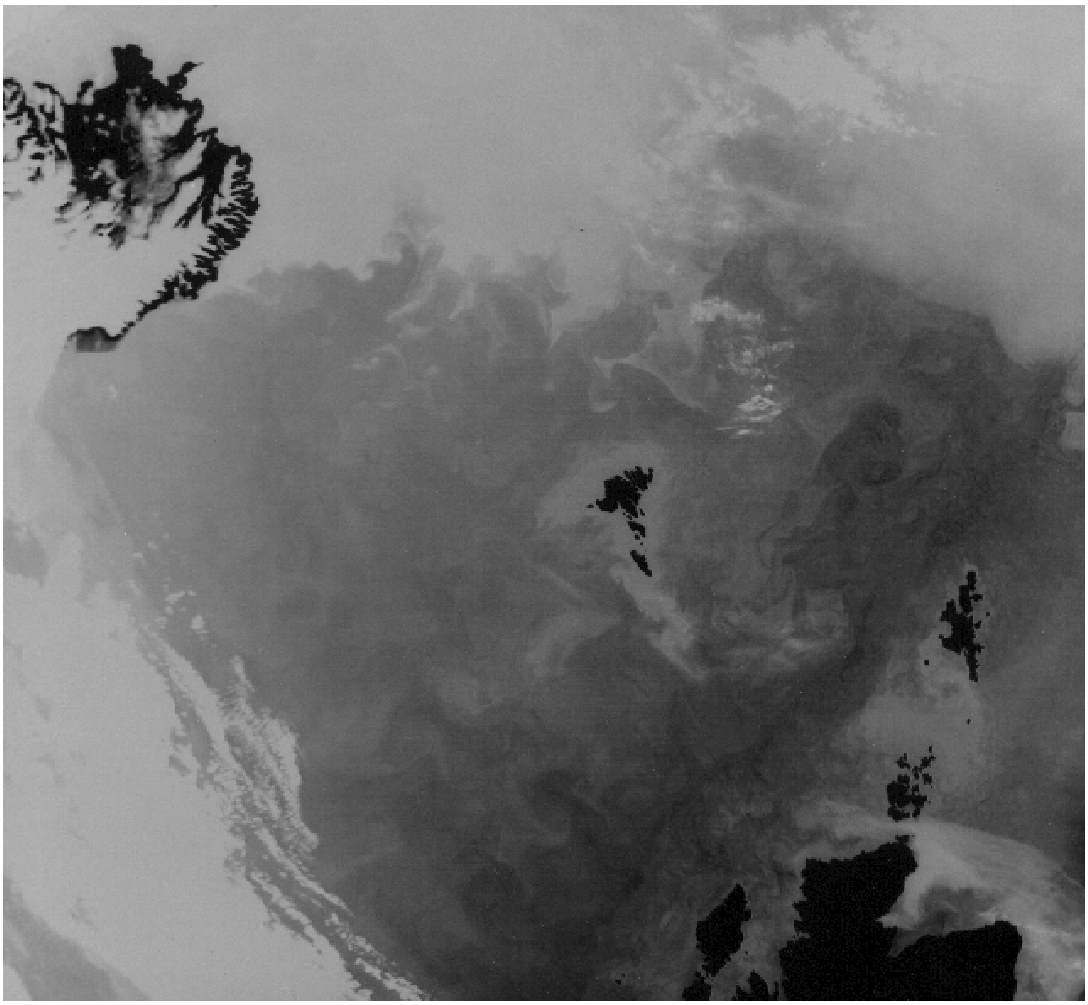

by

Karin Margretha Húsgarð Larsen

Geophysical Institute
Dept. of Physical Oceanography
University of Bergen

Faroese Fisheries Laboratory
Environmental dept.

May 2003

Abstract

The water mass on the Faroe Shelf is distinct from the off-shelf water surrounding the shelf. This difference of water masses is reflected in the temperature and salinity distributions. The on-shelf water is colder and fresher than the off-shelf water throughout most of the year. A temperature/salinity front thus forms, where the on-shelf water meets the off-shelf water. The waters inside the front have a different cycle of primary production and support a different ecosystem from the off-shelf waters and they are important nursery areas for larvae of many commercially important fish stocks. Sea surface temperature measurements from the R/V Magnus Heinason in the period February 1999 to November 2000 show the existence of the front throughout the year except for a short period in autumn, and the largest cross-frontal gradients are found in the spring. Also, the measurements are used to find typical values for the frontal location and width in various directions across the shelf. The observed characteristics of the front are discussed in relation to bottom topography and proximity to a shelf edge, to the heating/cooling cycle driven by the air-sea heat flux, and to various theories for fronts generated by tidal mixing.

Acknowledgements

I would like to thank my supervisor at the University of Bergen, Prof. Harald Svendsen, at the Geophysical Institute for his helpful advices and suggestions throughout my work with this thesis. I would also like to thank my external supervisor Dr. Bogi Hansen at the Faroese Fisheries Laboratory. Without his help and guidance, I would not even have started this education.

Also, I want to thank Dr. Knud Simonsen for letting me use data from his tidal simulation of the Faroe Shelf and for other help through this work.

I would also like to thank the Faroese Fisheries Laboratory and especially its director Hjalti í Jákupsstovu for letting me do my thesis work there. Thanks to all my colleagues for help, support and for a good working environment.

Although not directly related to this thesis work, I would like to thank Svein Østerhus and his wife for inviting me to stay at their home in Bergen, and thanks Svein for letting me disturb you at your office at Geophysical Institute every time I had errands at the Institute.

Finally, I owe the deepest thanks to my husband Aksel for his patience and for his support during my years of studying. Thank you for encouraging me when things looked too chaotic. I also want to thank my family for their support and for taking care of our children, when I and Aksel were respectively abroad and at sea.

Tórshavn 24-05-2003

Karin Margretha Húsgarð Larsen

Contents

1 Introduction

The Faroe Islands are located on the Greenland-Scotland Ridge between Iceland and Scotland. Because of the key position in North Atlantic – Nordic Seas exchanges, a large number of expeditions have been in the area, but most of them have been concentrated on the off-shelf circulation (e.g. Overflow '60 and Overflow '73). A few of the old expeditions however, have been made partly on the shelf. For instance, already in the first decade of the 20'th century Knudsen (1905) analysed temperature and salinity measurements made by the mailsteamer "Laura" in the years 1897 – 1904 on her routes from Denmark to Iceland or Greenland, via the Faroe Islands. The results show both lower temperatures and lower salinities in the Faroe Shelf area than offshore. Also the research steamer "Thor" was in the Faroe area in May – June 1910. On this cruise, a section was made from west of Suduroy (southern most island of the Faroes) and crossing the Faroe Bank Channel and the Faroe Bank. The station closest to Suduroy showed a mixed water column with low temperatures and salinities (Knudsen, 1911). Both of these investigations thus indicate the properties of the water mass on the shelf. A more precise description of the shelf water properties and distribution was given by Ellet and Debrah (1974) and the actual existence of a shelf front is observed by Hansen (1979 and 1992). In recent years, the Faroese Fisheries Laboratory has arranged annual biological/oceanographic surveys on the Plateau, besides other hydrographic surveys, which partly are made on the Plateau. Finally, there exists a long temperature time series from the coastal station Mykines, which extended from 1914 to 1969. It is reported by, for instance Smed (1953) and Hansen (2000).

Biologically the shelf water is of great importance. Several plankton and 0-group surveys are made on the Faroe Plateau and, for instance Fraser (1949) finds, that the plankton composition on the shelf is quite different from the off-shelf composition. Also, a figure by Bertelsen (1951) shows, that cod larvae are more abundant on-shelf than off-shelf. More recently, Gaard et. al. (2002) show, that primary production on the Faroe Shelf correlates remarkably well with recruitment and mean weight of cod and haddock on the Faroe Plateau. Also, the primary production is seen to have a high interannual variability, but with a period of several years (Gaard et. al., 2002). The observed variability in primary production can partly be explained by variation in grazing pressure, which is dominated by the biomass of *Calanus finmarchicus* (Gaard et. al., 1998). Since *Calanus* is an oceanic species, it enters the shelf water in the spring through inflow of off-shelf water. A relationship between inflow and *Calanus* is described by Gaard and Hansen (2000), but more detailed knowledge about the front and the inflow and variations thereof are required to get a better understanding of the possible processes, that determine shelf production.

Fronts at other locations similar to the Faroe Shelf have been under intensive studies since the mid seventies, e.g. at the Georges Bank (e.g. Loder and Greenberg, 1986; Drinkwater and Loder, 2001) and around the British Isles (e.g. Simpson and Hunter, 1974; Fernhead, 1975; Soulsby, 1983). These studies have resulted in the proposal of several frontal theories, some of which will be tested in this thesis.

The objectives of this thesis are to determine the characteristics of the Faroe Shelf Front (e.g. location and cross frontal temperature difference) and investigate which processes influence the characteristics seasonally or in a fortnightly period.

Following this introduction, Chapter 2 describes the Faroe Shelf and its surroundings, including description of the topography, oceanography and atmospheric forcing. Then Chapter 3 follows, with description of theories related to shelf fronts. In Chapter 4, the Sea Surface Temperature data used in this thesis are described, and in Chapter 5 the results of these data are presented. In Chapter 6 a heat budget for the Faroe Shelf and its surroundings is calculated in trying to reproduce the observed seasonal temperature variation on-shelf and off-shelf. In Chapter 7, the observed frontal location is compared to the frontal location predicted by theories. Hereafter, a discussion is given in Chapter 8, followed by a summary and concluding remarks in Chapter 9.

In Appendix A, a table lists the characteristics of the Sea Surface Temperature data, while Appendix B describes the tidal simulation, which is used for the theoretic predictions.

2 The Faroe Shelf and its surroundings

2.1 Topography

The Greenland-Scotland Ridge separates the North Atlantic from the Nordic Seas, and on this ridge the Faroe Islands are situated between Iceland and Scotland (Fig 2.1). The Greenland-Scotland Ridge is mainly shallower than 300 m, but there are some deep passages across, especially in the Denmark Strait, which has a sill depth of 620 m and in the Faroe Bank Channel with a sill depth of 840 m. The crest of the Iceland-Faroe Ridge is 480 m at the deepest point, but is mainly between 300 and 400 m deep. The deepest part of the Wyville-Thomson Ridge crest is approx. 600 m.

South of Iceland is the Iceland Basin, which is mostly deeper than 2000 m. It is bounded to the north west by the Reykjanes Ridge and to the south east by the Rockall-Hatton Plateau. The Faroe-Rockall Plateau, which is the ridge from the Faroes to the Rockall Bank, is mainly between 1000 and 1500 m, but it also includes some banks. These are, starting south west of the Faroe Plateau: the Faroe Bank, the Bill Baileys Bank, the Lousy Bank, the Hatton Bank, and the Rockall Bank. A very small area of the Rockall Bank is above the surface and is called the Rockall. Between the Rockall Bank and the Scottish and Irish Shelf, is the Rockall Channel, which is more than 2000 m deep.

North of the Faroes is the Norwegian Basin, which is deeper than 3000 m. South east of the Faroes is the Faroe-Shetland Channel, which enters the Norwegian Basin to the north. The Faroe-Shetland Channel is almost everywhere deeper than 1000 m. It rounds the southern tip of the Faroe Plateau, where it meets the Wyville-Thomson Ridge to the west and then turns north westwards. The remaining part of the Channel, which is between the Faroe Plateau and the Faroe Bank is called the Faroe Bank Channel. There is no distinct border between the Faroe-Shetland Channel and the Faroe Bank Channel.

Figure 2.2 shows the topography of the Faroe Plateau in more details. The shelf area is usually considered to be within the 150 m or 200 m bottom contour (Larsen *et. al.*, 2002; Hansen, 2000). The 150 m contour roughly describes a triangle with a long and narrow corner pointing to the south. The width of the shelf is thus variable, being only about 12 km wide east of the southernmost island and about 50 km wide in the north western direction, where the Iceland-Faroe Ridge encounters the Faroe Plateau.

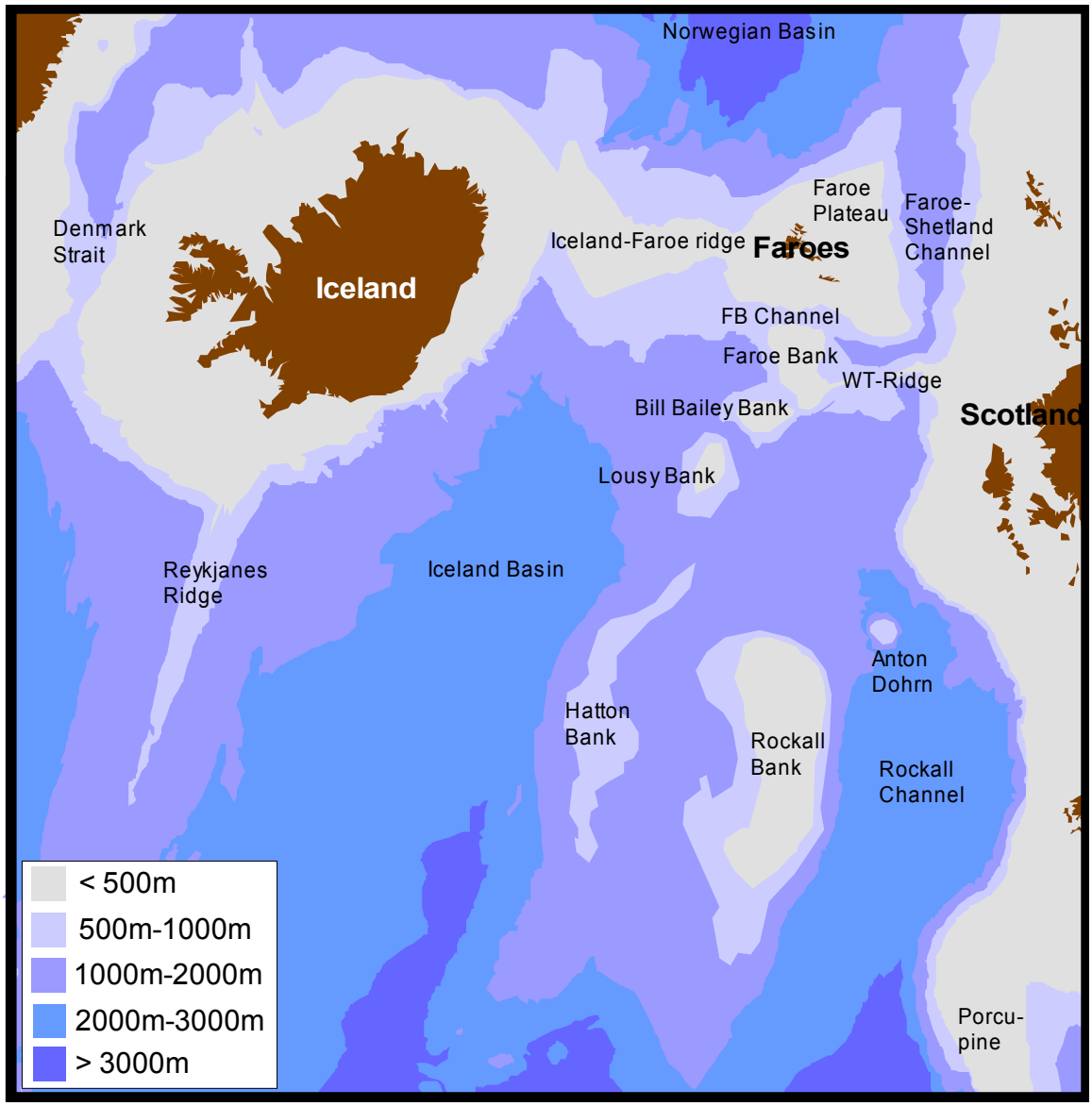

Figure 2.1 The topography of the Northern North Atlantic, showing the Greenland-Scotland Ridge and the basins and plateaus to the south and to the north of the ridge. From Hansen, 2000.

Table 2.1 The table lists different areas on the Faroe Plateau. In the first column is listed a depth interval, and the area in between these intervals is listed in the second column. The third column lists depth contours and the related areas above these contours (including land) are listed in column four. From Hansen, 2000.

Depth (m)	Area (km^2)	Depth (m)	Area (km^2)
0 – 100	5300	Above 0	1400
100 – 200	14700	Above 100	6700
200 – 300	12000	Above 200	21400
300 – 400	5300	Above 300	33400
400 – 500	5700	Above 400	38700
		Above 500	44400

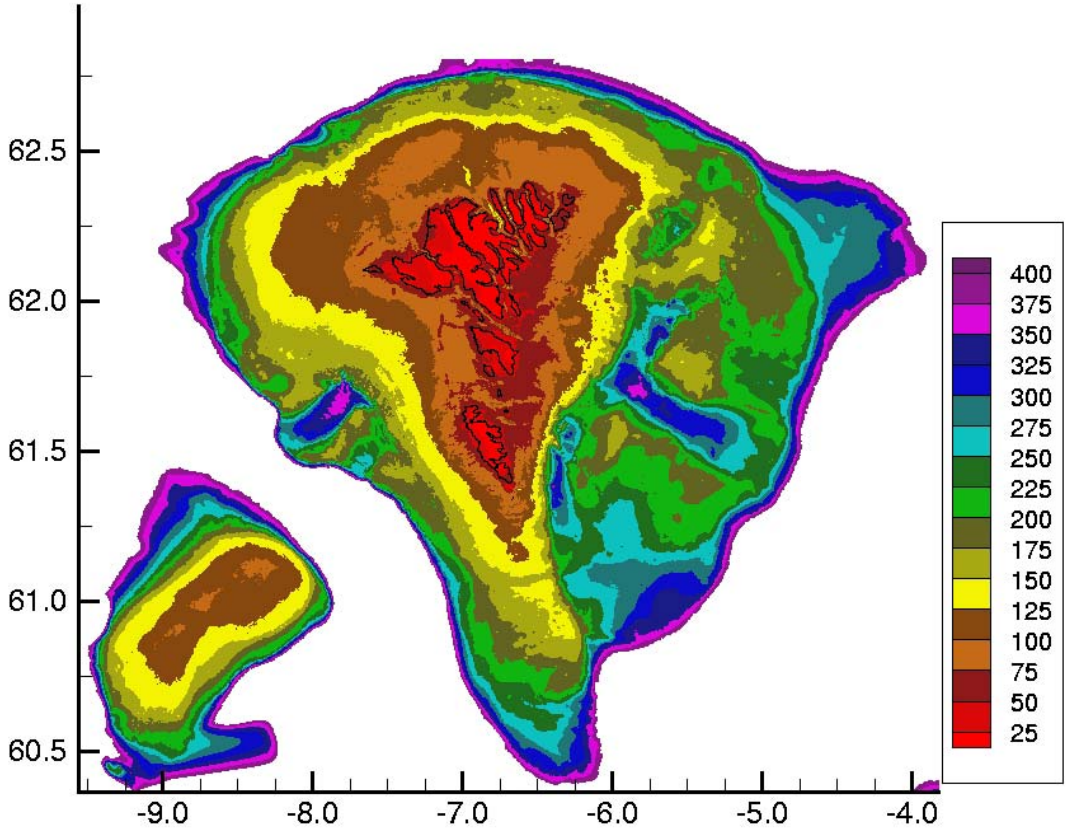

Figure 2.2 The topography on the Faroe Plateau and the Faroe Bank. By courtesy of Knud Simonsen.

Almost everywhere around the Faroe Plateau, the bottom depth exceeds 1000 m except for the shallowest parts of the Faroe Bank Channel west of the Plateau and the Iceland-Faroe Ridge area to the northwest. To the east on the Plateau there are some banks separated by canyons and also one bank to the west, but these areas are not considered as a part of the Faroe shelf area although they are shallower than 200 meters.

In Table 2.1 are listed areas related to different depths on the Faroe Plateau. The area between 100 and 200 m depth is largest, but in Figure 2.2 it is seen, that the area between 75 and 100 m also has a large contribution to the shelf area.

2.2 Large-scale circulation in the Faroe region

In the upper layers in the Faroe region, the North Atlantic Current (NAC) flows from south west on the northern slope of the Faroe-Rockall Plateau (Fig. 2.3). Here it splits

into two branches, one flowing south of the Faroes through the Faroe-Shetland Channel and the other flowing northwards and crossing the Iceland-Faroe Ridge at various locations.

After crossing the Iceland-Faroe Ridge, the Atlantic water is focused in the Faroe Current (FC), which flows north of the Faroes. In passing the northeast corner of the Faroe Plateau, the FC splits into two branches. One flows southwards into the Faroe-Shetland Channel, where it turns and joins the NAC branch flowing south of the Faroes. The other branch continues into the Norwegian Sea, where it recirculates. In addition to the NAC, the Continental Slope Current (CSC) flows along the Scottish continental slope, bringing heat and salt into the Nordic and Arctic Seas. The water mass in the NAC is termed Modified North Atlantic Water (MNAW), while the water mass in the CSC is termed North Atlantic Water (NAW). Their characteristics are given in Table 2.2.

North of the Iceland-Faroe Ridge, the MNAW meets the East Icelandic Current (EIC). On the border between these flows, is the Iceland-Faroe Front (IFF), where Modified East Icelandic Water (MEIW) is formed. The MEIW is fresher and colder than the MNAW (Table 2.2) and it sinks below the MNAW. The EIC is therefore seen in the surface close to Iceland only, but continues below the surface along the northern slope of the Iceland-Faroe Ridge (Fig 2.3).

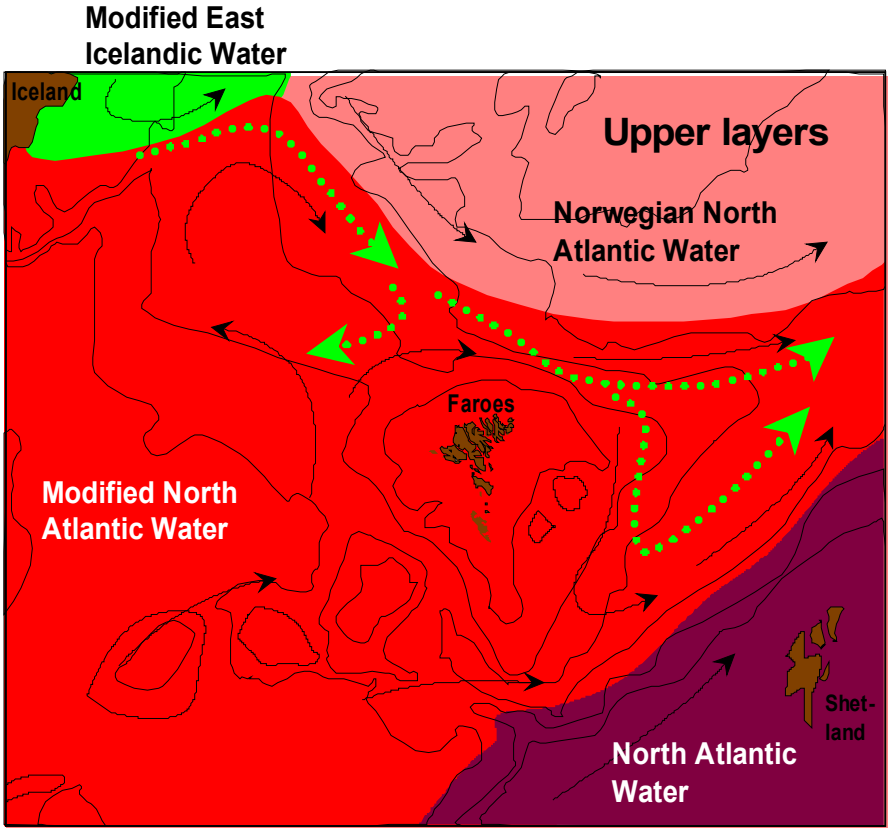

Figure 2.3 Circulation in the upper layers. Black arrows indicate direction of main surface currents, while dotted green arrows indicate the paths of the East-Icelandic Current after sinking below surface in the frontal area. Adapted from Hansen, 2000.

Table 2.2. Typical properties of the main water masses in the Faroe region. Adapted from Hansen and Østerhus, 2000.

Acronym	Name	Temperature range	Salinity range
MNAW	Modified North Atlantic Water	7.0 – 8.5°C	35.10 – 35.30
NAW	North Atlantic Water	9.5 – 10.5°C	35.35 – 35.45
MEIW	Modified East Icelandic Water	1.0 – 3°C	34.70 – 34.90
NSAIW	Norwegian Sea Arctic Intermediate Water	-0.5 - +0.5°C	34.87 – 34.90
NSDW	Norwegian Sea Deep Water	< -0.5°C	34.91

In the Nordic Seas and the Arctic Ocean, dense water, characterised as either deep or intermediate water, is formed by convective or other sinking processes. These waters need to outflow somewhere and this outflow is greatly affected by the Greenland-Scotland Ridge, which forms a barrier between the North Atlantic and the Nordic Seas. The basins north of the ridge are filled with dense water. These waters spill over the ridge and are therefore termed “overflow waters”.

There are three water masses in the overflow water crossing the Iceland-Scotland Ridge. These are MEIW, which, as mentioned, is produced in the frontal zone north of the ridge, Norwegian Sea Arctic Intermediate Water (NSAIW), which is produced in the Nordic Seas and finally, Norwegian Sea Deep Water (NSDW), which is found in the deepest parts of the Norwegian Basin, and is believed to originate from deep convection in the Greenland Sea and from shelf convection around the Arctic Ocean.

The overflow crossing the Iceland-Faroe Ridge includes all three overflow water masses. The MEIW is found between the MNAW inflow in the upper layer and the NSAIW and NSDW in the bottom layer. Also higher concentrations of MEIW are found close to Iceland, while NSAIW and NSDW seem to have the largest influence in the Faroese end of the ridge. NSAIW and NSDW tend to flow close to the bottom in several overflow branches associated with depressions in the Iceland-Faroe Ridge (Fig. 2.4).

Most of the overflow, which crosses the Iceland-Scotland Ridge, flows through the Faroe-Shetland Channel and continues through the Faroe Bank Channel, since this is the deepest passage in the ridge. All three overflow water masses are found in the Faroe-Shetland Channel, but the MEIW is believed to recirculate in the Channel (Fig. 2.3) and thus only small indications of MEIW are found in the overflow water of the Faroe Bank Channel, which is generally considered to consist of NSAIW and NSDW.

Finally some overflow crosses the Wyville-Thomson Ridge, intermittently both in space and time. This overflow is mainly confined to the depression in the middle of the ridge, but also to the ridge crest northwest of the depression. Nonetheless, evidence of intermittent overflow is also found over the southern part of the Wyville-Thomson Ridge.

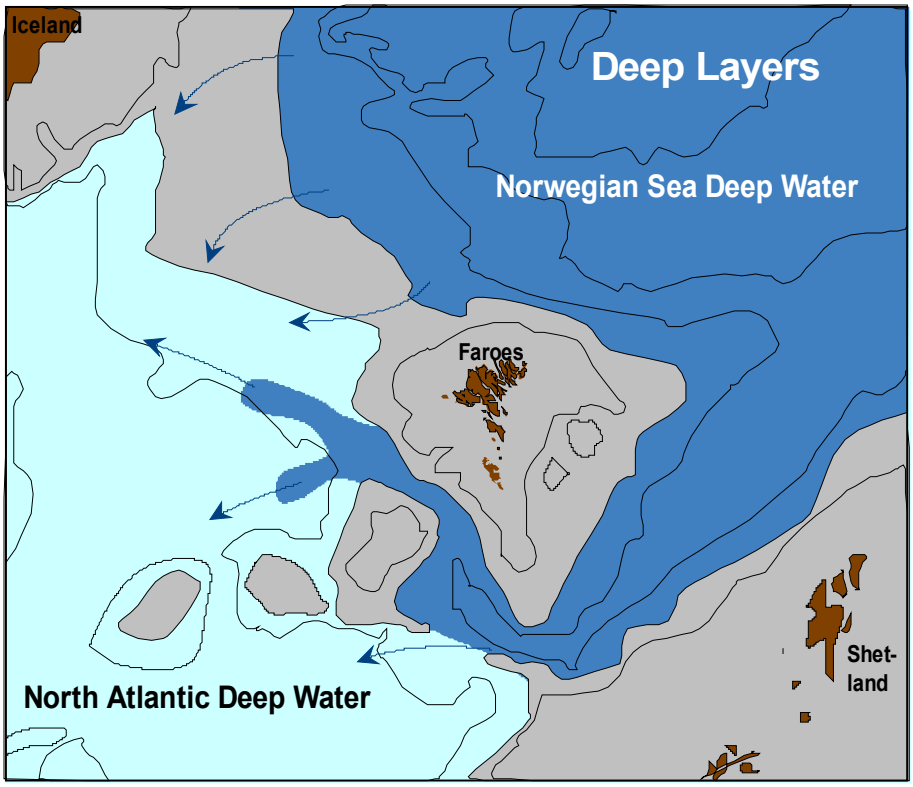

Figure 2.4. Circulation in the deeper layers. The dark blue colour indicates overflow water colder than 0°C. Light blue colour indicates North Atlantic Deep Water with temperature between 2 and 3°C close to the bottom. Arrows indicate the paths of the overflow water crossing the Iceland-Scotland ridge. Adapted from Hansen, 2000.

2.3 Oceanography of the Faroe Shelf

The oceanography on the Faroe Shelf is dominated by strong tidal currents. The tides mix the shelf water almost completely and convert it into a homogeneous water mass termed Faroe Shelf Water (FSW) (Hansen et al., 1998). The FSW is fresher and colder than the surrounding water mass, which mainly consists of MNAW. On the border between the FSW and the MNAW, there is a front, termed the Faroe Shelf Front. Cross frontal temperature differences are on the order of one degree C (Hansen, 1992), while cross frontal salinity differences are between 0.05 and 0.2 (Hansen et al. 1998). This produces typical density differences of 0.1 kg m^{-3} with denser water on-shelf. Figure 2.5 shows typical temperature and salinity distributions on the Faroe Shelf.

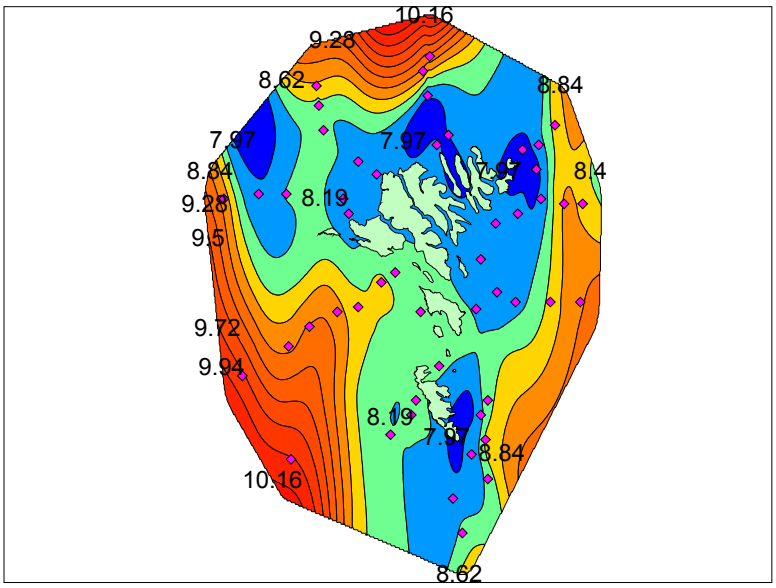

(a)

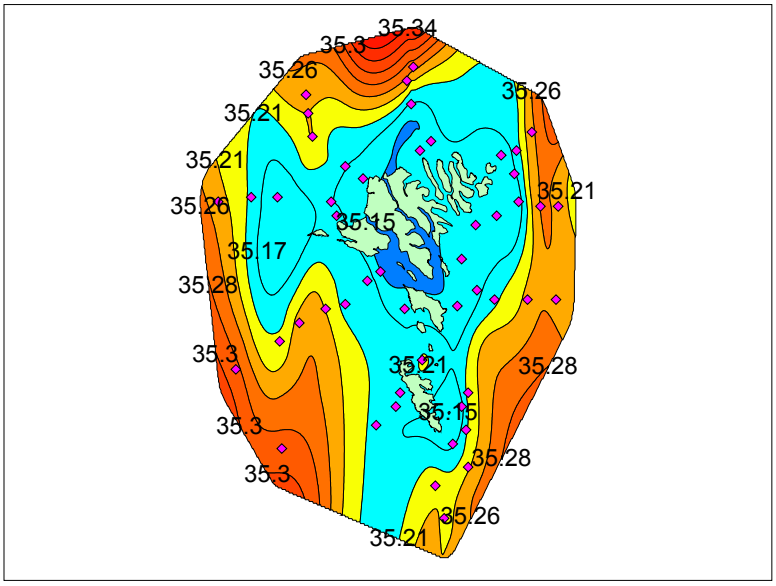

(b)

Figure 2.5. Temperature (a) and salinity (b) distribution at 20 m depth on the Faroe Shelf, 18-29 June 1999. Pink dots indicate CDT stations. Contours are created in MapInfo.

The seasonal temperature variation on the shelf has a greater amplitude than the off-shelf temperature variation (Fig. 2.6). Actually, the on-shelf water becomes warmer than the off-shelf water at 100 m depth in the summer months, but the net air-sea heat flux at these latitudes is not sufficiently large to make the on-shelf water warmer than the off-shelf surface water, as is seen on Georges Bank (Loder et. al., 1982; Mavor and Bisagni, 2001). On the other hand, the effective cooling of the shelf water during autumn and winter cause the pronounced shelf front observed in February and March, before the onset of off-shelf stratification (Fig. 2.6).

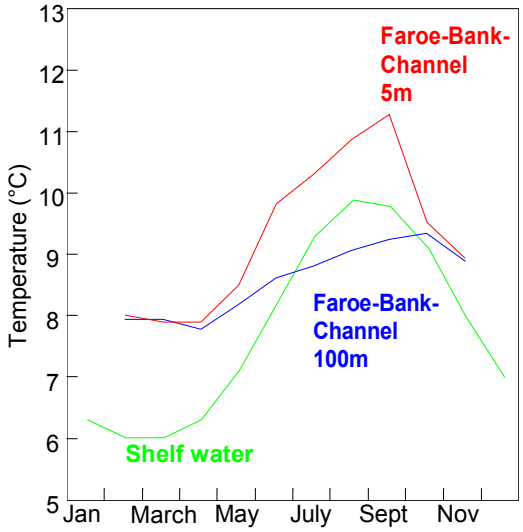

Figure 2.6. Monthly mean temperature (°C) on the shelf (green) and in the Faroe Bank Channel at 5 m depth (red) and 100 m depth (blue) representing off-shelf water. The temperature on the shelf is based on measurements at Mykineshólm 1914-69, while the temperatures in the Faroe Bank Channel are based on measurements from R/V Magnus Heinason 1982-97. Adapted from Hansen, 2000.

Because of the proximity of an amphidrome north of the Faroes and a degenerate amphidrome on the islands, the tides on the shelf are rather complicated. Figure 2.7 shows the time lag and range for the M_2 tidal heights around the Faroes. In Figure 2.7 it is seen, that the tidal wave comes in from the west and then flows north and south of the Faroes.

Current speeds on the Shelf are typically on the order of one m/s, but may between the islands be several meters per second (Simonsen, 1999). In the fjords, the current speeds generally are smaller and typical maximum values here are between 0.2 and 0.3 m/s (Larsen, 1999).

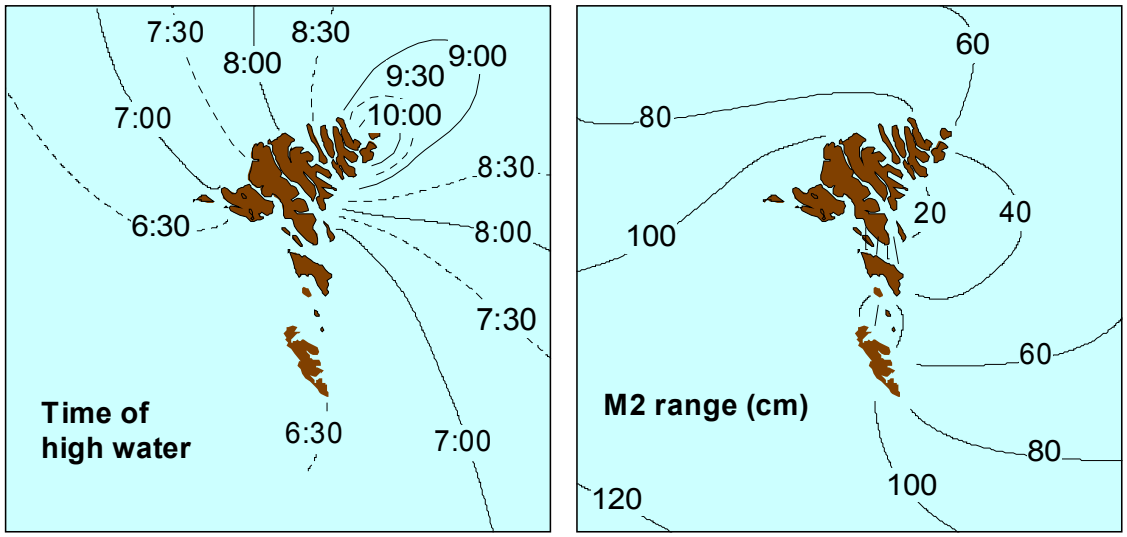

Figure 2.7. Tidal chart of the Faroese region for the M_2 heights. The left figure shows the time lag (in hours) of high water after the moons passage over Tórshavn. The right figure shows the M_2 range (twice the amplitude) in cm. The small ranges close to land east of the islands indicate a degenerate amphidrome. From Hansen, 2000 (based on work by Knud Simonsen).

On the Shelf there is a persistent anticyclonic circulation, where the residual currents follow the depth contours (Fig. 2.8). Tidal rectification is believed to have a large contribution to the residual flow, but also ocean currents may have some influence together with meteorological forcing (Hansen, 1992). The direction of the residual flow is at most locations very steady, but at some locations there are indications of a seasonal variation in both residual speed and direction. Figure 2.8 shows residual currents at selected locations on the shelf.

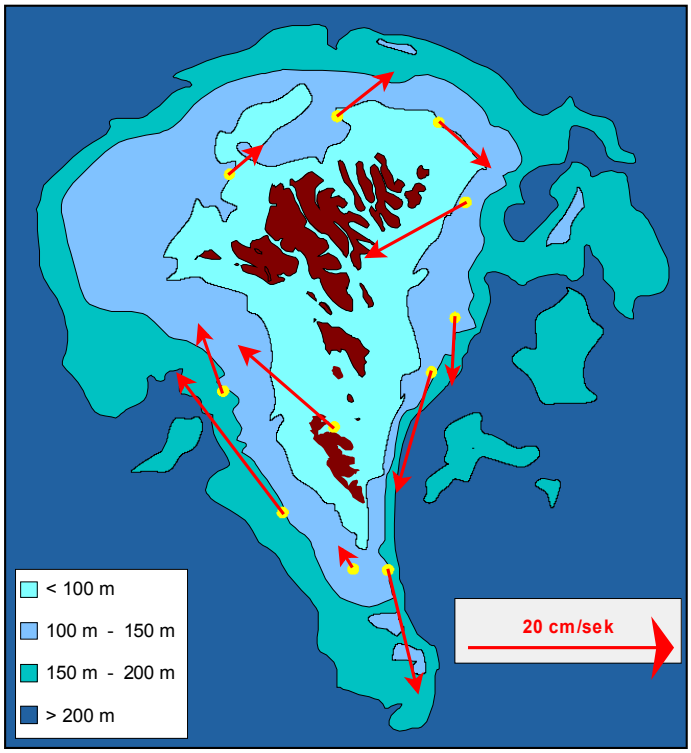

Figure 2.8. Residual currents on the Faroe Shelf at 20 to 40 m depth. Yellow circles show position of current measurements. Residual speed and direction is indicated by red arrows. From Hansen, 2000.

2.4 Atmospheric forcing

The climate on the Faroe Islands is greatly influenced by the passing of frequent cyclones, which have a main track close to the islands from south westerly directions. The Faroe Islands are thus generally considered as windy with highest mean wind speeds during winter (6.5 – 10 m/s). The most frequent wind direction is from southwest, while east is the most infrequent wind direction (Cappelen and Laursen, 1998).

Monthly mean air temperatures have only small differences between summer and winter. January and February are the coldest months with monthly mean temperatures around 3.5°C, while July and August are warmest with a monthly mean of approximately 10.5°C (Cappelen and Laursen, 1998).

The yearly average net air-sea heat flux in the Faroese region is between –80 and –40 W/m^2. Thus in average the sea looses heat to the air, but this is compensated for by the warm NAC. Monthly mean net air-sea heat flux is positive only for the months May to August (Lindau, 2001).

As mentioned in the previous section, the FSW is fresher than the surrounding off-shelf waters. The reason for this is a combination of the increased precipitation over the islands compared to over the sea and the smaller volume of FSW due to the shallow shelf. The normal annual precipitation in Torshavn is 1284 mm, with largest total precipitation during autumn and winter. Geographical variations are seen in the annual precipitation ranging from approx. 800 mm to above 3000 mm at specific locations (Cappelen and Laursen, 1998). Gaard and Hansen (2000) used the precipitation over land to estimate the flushing rate of FSW. In their calculations, they assumed the annual precipitation minus evaporation over the shelf water, plus river runoff from land to be between 500 and 1500 mm.

3 Frontal theories

In the open ocean, variables such as temperature and salinity are usually not varying gradually in the horizontal direction. Over large areas, horizontal gradients are small. These areas can be bounded by a thin region with large gradients, defined as a front. The frontal region can be dominated by large temperature or salinity gradients, which is reflected in large density gradients also, indicating an along front flow. If the front is reflected in both temperature and salinity, they may compensate each other, resulting in only small or no variation in density.

In the open ocean, fronts are typically found where ocean currents meet. In coastal areas fronts can be found at shelf breaks, in areas with strong tidal currents and in coastal upwelling areas. In this chapter two main theories on tidal fronts are described and also the shelf break front.

3.1 H/U^3

Simpson and Hunter (1974) established a frontal theory based on energetic considerations. They postulated, that if an amount of heat is added at the surface, this heat adds buoyancy to the surface water. To overcome this buoyancy and mix it throughout the water column you need a certain amount of turbulent energy, in this case assumed supplied by the tide. The position of the front (Fig 3.1) will then be, where the tidal energy is large enough to mix the added buoyancy at the surface through the whole water column.

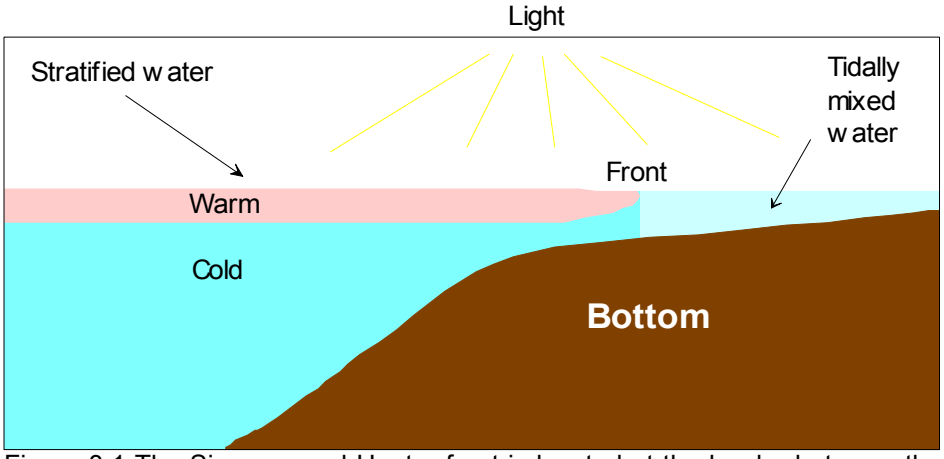

Figure 3.1 The Simpson and Hunter front is located at the border between the stratified off-shelf water and the mixed on-shelf water. From Hansen, 2000.

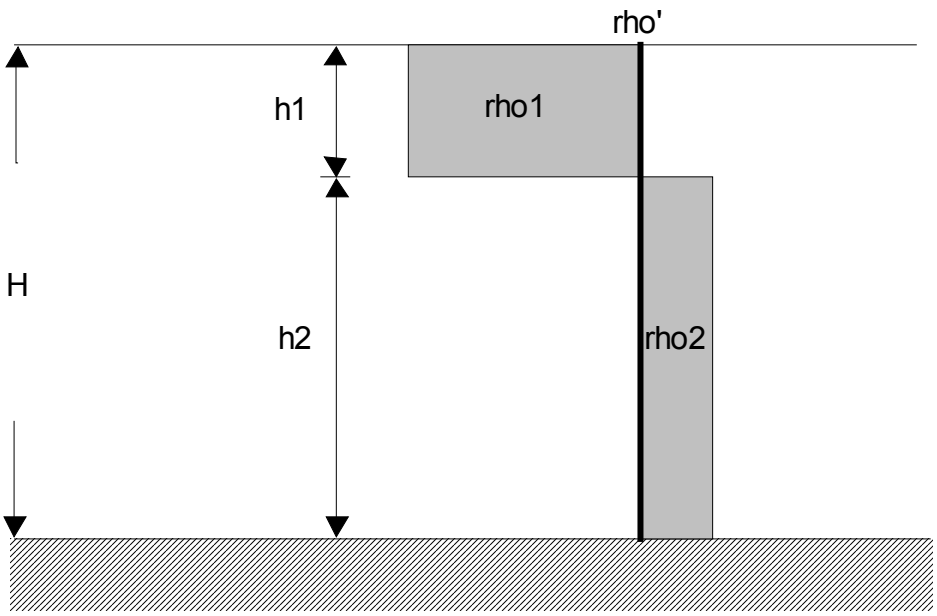

Figure 3.2. In the stratified case, the water column consists of an upper layer with height h1 and density rho1, and a lower layer with height h2 and density rho2 indicated by the two grey rectangles of assumed equal area. After mixing, the water column is homogeneous with density rho' indicated by the thick vertical line.

The following reproduction of the theory is based on Mann and Lazier (1996), Simpson and Hunter (1974), and Loder and Greenberg (1986). The calculations are done by considering the potential energy of the stratified water column versus that of the mixed column. The potential energy above one m^2 of seabed for the stratified water column is (Fig. 3.2):

$$PE_{str} = \rho_1 g h_1 \left(\frac{h_1}{2} + h_2 \right) + \rho_2 g h_2 \left(\frac{h_2}{2} \right) \qquad (3.1)$$

where ρ_1 and ρ_2 (kg m^{-3}) are the densities of the upper and lower layer, respectively, g (m s^{-2}) is the gravitational acceleration, h_1 and h_2 (m) are the thickness of the upper and lower layer, respectively, and the expressions in the brackets are the centre of mass of the upper and lower layer, respectively. Similarly the potential energy for the mixed water column can be expressed as:

$$PE_{mix} = \frac{1}{2} \rho' g (h_1 + h_2)^2 \qquad (3.2)$$

where ρ' is the density of the mixed water. Since the mass is conserved within the water column, ρ' can be expressed with ρ_1 and ρ_2 and PE_{mix} can be rewritten as:

$$PE_{mix} = \frac{1}{2} g(\rho_1 h_1 + \rho_2 h_2)(h_1 + h_2) \qquad (3.3)$$

The difference in potential energy between the two states becomes:

$$\Delta PE = PE_{mix} - PE_{str} = \frac{1}{2} g h_1 h_2 (\rho_2 - \rho_1) \qquad (3.4)$$

Since ρ_2 is larger than ρ_1, this quantity is positive, meaning that we have to add energy to get from the stratified state to the mixed state. This added energy is assumed supplied by tidal currents by the generation of turbulent energy, D_t (W m^{-2}), at the bottom. Assuming, that only a fixed fraction, ε_t, of the turbulent energy is used to mix the water, the rate of added energy can be written as:

$$\varepsilon_t D_t = \varepsilon_t \rho C_d U^3 \text{; where } U^3 = \left\langle \left(u^2 + v^2\right) \right\rangle^{3/2} \qquad (3.5)$$

C_d is the bottom drag coefficient, u and v (m s^{-1}) are the east and north tidal current components, respectively and the angle brackets denote a fortnightly tidal average.

Using the assumption, that $h_1 << h_2 \Leftrightarrow h_2 = H$, where H is the bottom depth and further that the fractional density change is a linear function of temperature it follows

$$\frac{\rho_2 - \rho_1}{\rho} = \frac{\Delta\rho}{\rho} = \alpha \Delta T \Leftrightarrow \Delta\rho = \alpha\rho\Delta T = \frac{\alpha\rho Q \Delta t}{m C_p} \qquad (3.6)$$

where α (°C^{-1}) is a constant, Q (W m^{-2}) is the heat input at the surface, Δt (s) is the time interval necessary to increase the temperature ΔT, m (kg m^{-2}) is the mass of the upper layer and C_p (J Kg^{-1} °C^{-1}) is the specific heat of seawater. It is assumed, that the only heat source is a heat input at the surface. Substituting Eq. 3.6 into Eq. 3.4, replacing m with ρh_1, using the assumptions made above and converting Eq. 3.4 into a rate of supplied potential energy, results in:

$$\frac{\Delta PE}{\Delta t} = \frac{gH\alpha Q}{2C_p} \qquad (3.7)$$

Since this is the energy rate necessary to keep the water column mixed, then everywhere, where the fraction of the turbulent energy rate given by Eq. 3.5 is larger than given by Eq. 3.7, the water will be mixed out to the border, where they are equal:

$$\varepsilon_t D_t = \frac{gH\alpha Q}{2C_p} \Leftrightarrow \frac{H}{D_t} = \frac{2C_p \varepsilon_t}{g\alpha Q}; \qquad (3.8)$$

The front will then be located, where Eq. 3.8 is fulfilled.

This theory is based on some assumptions or simplifications. For instance ε_t, the fraction of the turbulent energy available for work against gravity, is considered constant. None the less, the value for ε_t varies somewhat in literature, but is generally on the order of 10^{-3}. (Loder and Greenberg, 1986; Simpson, 1998). An improvement of the theory is tested by Simpson and Bowers (1981), where they suggest, that ε_t is a function of the actual stratification (i.e. ε_t decreases as stratification increases). Another possibility might be, that ε_t is a function of the tidal velocity. If U^3 is twice as large at location 1 compared to location 2, is the available kinetic energy at location 1 necessarily also twice as large compared to location 2? If not, we should expect to find, that one value for ε_t fits well at one location, but not at another, where the tidal velocity is different.

3.2 H/U – Boundary layers

The H/U theory is based on surface and bottom boundary layers, where the bottom boundary layer arises from tidal streams, while the surface boundary layer arises from wind. The H/U front is located where the two layers added occupy the whole water column (Fig. 3.3). On the on-shelf side of the front, the water column will be completely mixed, while it can be stratified on the off-shelf side. These boundary layers are widely discussed in literature, especially the bottom boundary layer, since the wind mixed layer often is neglected. In this thesis, only the bottom boundary layer is included, while the wind mixed layer is left to future investigations.

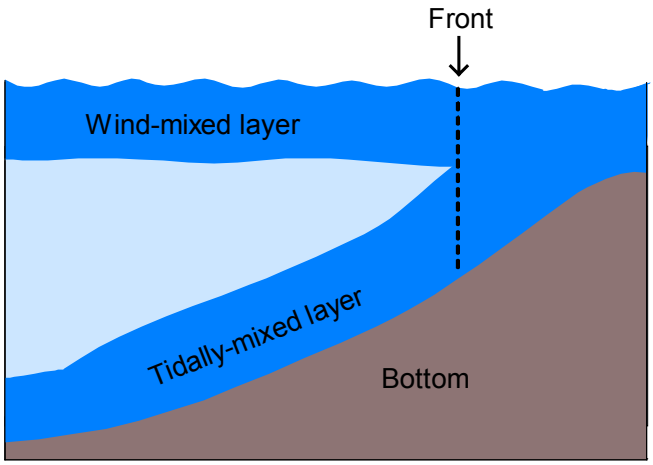

Figure 3.3. The H/U front is located where the boundary layers add up to occupy the whole water column.

Soulsby (1983) identifies seven different bottom boundary layers restricted to different conditions. He implies, that in practice, the boundary layer may be a combination of several of the idealised layers. The planetary boundary layer also called the Ekman layer, where the bottom friction, influenced by the rotation of the earth, creates a bottom boundary in a steady current, is widely used (Loder and Greenberg, 1986; Stigebrandt, 1988). The thickness of this layer is given as:

$$\delta_U = \frac{C\sqrt{C_d}U}{f} \qquad (3.9)$$

where C is a constant, f (s^{-1}) is the local Coriolis parameter, C_d is the bottom drag coefficient, and $U = \left\langle \left(u^2 + v^2\right) \right\rangle^{1/2}$ (m s^{-1}).

If the current, on the other hand, is oscillating with the frequency ω (s^{-1}), then the boundary layer is given by:

$$\delta_O = \frac{C\sqrt{C_d}U}{\omega} \qquad (3.10)$$

This could be tidal currents, where the oscillating frequency then equals the frequency of the tidal constituent.

Soulsby (1983) implies, that the planetary boundary layer is valid mainly for steady and unbounded deep flows, while the oscillatory boundary layer is valid for rectilinear tidal currents in channels or near coastlines. On shelves, on the other hand, both the planetary and the oscillatory boundary layers are important, and the resultant boundary layer is a combination of the two. The tidal ellipse can be decomposed into two counter rotating vectors of constant (but not necessarily equal) length – one cyclonic (R_+) and one anticyclonic (R_-) both with frequency ω. The boundary layer thickness of the combined planetary and cyclonic and anticyclonic rotations, respectively then are given by:

$$\delta_+ = \frac{C\sqrt{C_d}U}{\omega + f} \text{ and } \delta_- = \frac{C\sqrt{C_d}U}{\omega - f} \qquad (3.11)$$

In the northern hemisphere, the anticyclonic layer will always be larger than the cyclonic layer, which suggests, that the thickness of the mixed layer is equal to the thickness of the anticyclonic layer. But here we have to take into account the rotation of the tidal ellipse. Soulsby (1983) suggests weighting these two layers by the relative length of the cyclonic and anticyclonic vectors. The thickness of the combined boundary layer then becomes:

$$\delta = \frac{|R_+|\delta_+}{|R_+| + |R_-|} + \frac{|R_-|\delta_-}{|R_+| + |R_-|} \qquad (3.12)$$

Substituting Eq. 3.11 into Eq. 3.12 and using $U_{maj} = |R_+| + |R_-|$ and $U_{\min} = |R_+| - |R_-|$ we find, that

$$\delta = C\sqrt{C_d}\,\frac{U_{maj}\omega - U_{\min} f}{\omega^2 - f^2} \qquad (3.13)$$

where U_{maj} and $U_{\min}$ are the major and minor semi-axis in the tidal ellipse, respectively. In areas, where the thickness of the boundary layer is greater than the bottom depth, the water column will be completely mixed. If, on the other hand, the boundary layer is smaller than the bottom depth the water column may be stratified. The front will be located where the boundary layer equals the bottom depth, i.e. where there is mixed water on the shallower side and may be stratified water on the deeper side.

3.3 Shelf-break front

Along the continental shelf break of, for instance the east coast of North America, there is a front separating the colder and fresher shelf water from the warmer and more saline off-shelf water (Mann and Lazier, 1996). This type of front is termed shelf-break front. Its existence is dependent on the tendency of the flow to follow isobaths. Its theory can therefore be related to the theory of conservation of potential vorticity, which is now to be reproduced here, based on Cushman-Roisin (1994). Assume a homogeneous frictionless barotropic flow. The horizontal equations governing such flow are:

$$\frac{Du}{Dt} - fv = -\alpha \frac{\partial p}{\partial x}; \qquad \frac{Dv}{Dt} + fu = -\alpha \frac{\partial p}{\partial y} \qquad (3.14)$$

where u and v (m s^{-1}) are the east and north velocity components respectively, f (s^{-1}) is the Coriolis parameter, α (m^3 kg^{-1}) is the reciprocal of density and p (N m^{-2}) is the pressure. Cross-differentiating these equations and subtracting results in:

$$\frac{D}{Dt}(f+\zeta) + \left(\frac{\partial u}{\partial x} + \frac{\partial v}{\partial y}\right)(f+\zeta) = 0; \quad \text{where } \zeta = \frac{\partial v}{\partial x} - \frac{\partial u}{\partial y} \qquad (3.15)$$

Here f and ζ are grouped, because they represent planetary and relative vorticity, respectively.

The continuity equation of volume is:

$$\frac{\partial h}{\partial t} + \frac{\partial}{\partial x}(hu) + \frac{\partial}{\partial y}(hv) = 0; \quad \text{where } h = H + \eta \qquad (3.16)$$

H (m) is the bottom depth and η (m) is the surface elevation. Differentiating the second and third term and rearranging, the continuity equation can be rewritten as:

$$\frac{D}{Dt}h + \left(\frac{\partial u}{\partial x} + \frac{\partial v}{\partial y}\right)h = 0 \qquad (3.17)$$

Combining equation 3.15 and 3.17 by eliminating the horizontal divergence term and using the derivation rule of a fraction results in:

$$\frac{D}{Dt}\left(\frac{f+\zeta}{h}\right)=0 \qquad (3.18)$$

If it is assumed, that $|\zeta| << f$ (neglecting velocity shear), $|\eta| <<$ H, $|\nabla\zeta|<<|\nabla f|$ and $|\nabla\eta|<<|\nabla H|$ we have that:

$$\frac{D}{Dt}\left(\frac{f}{H}\right)=0 \qquad (3.19)$$

This means, that the ratio (f/H) must be constant. In the f-plane (assuming constant f), H must also be constant and the current is "forced" to follow the bottom contours. This phenomenon is often called topographic steering (Pond and Pickard, 1986).

But this explanation might be too simple. Chapman (2000) argues, that over the shelf, bottom friction generates an appreciable boundary layer and the bottom friction can therefore not be excluded in the momentum equations. Also, since a jet often is associated with the front, relative vorticity might not be negligible compared to planetary vorticity and therefore our previous assumptions do not hold. In a simple barotropic model Chapman (1986) shows, how a shelf break front can be formed and maintained over a long distance. In this model temperature and salinity act as tracers, and because of convergence at the shelf break, a shelf-break front forms. In a newer model, including off-shelf stratification Chapman (2000) shows the importance of the bottom friction. Without the bottom friction no front is formed. Unfortunately there is no difference between a constant sloping shelf and a shelf with a shelf break, and Chapman's (2000) model therefore fails to explain the dynamics of the shelf break.

As described, the topographic steering and also Chapman's models (1986 and 2000) keep the shelf water on the shelf or within a critical depth. Because of run off, the shelf water is fresher than the off-shelf water, and during winter it is more effectively cooled because of the shallow depth. Because of the reduced exchange between the shelf and the off-shelf water, the fresher and colder shelf water is kept on the shelf and a front can form. A final comment on the shelf-break front is, that in the summer season at latitudes with sufficient solar radiation, the off-shelf water becomes stratified, while the stratification of the shelf water depends also on the bottom depth and the strength of tidal currents. If the shelf water becomes stratified, a "cold cushion" may form on the shelf break (Mann and Lazier, 1996; Allen et. Al., 1983). The shelf-break front thus still exists, but is now a sub-surface front and is not visible in the SST measurements.

4 Sea Surface Temperature – data and methods

4.1 Data material

In this work, sea surface temperature (SST) data measured by a research vessel logging system is used to map the front. The temperature measurements consist of 92 crossings of the Faroe Shelf Front by the R/V Magnus Heinason in the period February 1999 – November 2000. All months are represented, except for January and December. The R/V Magnus Heinason is equipped with a measuring system, where position (DGPS), bottom depth and SST at approx. 3 m depth are measured continuously and stored every 10 seconds. From these data, tracks crossing the 50 and 200 m depth contours and/or tracks with continuously increasing (or decreasing) depth between 50 and 200 m have been selected. These tracks are plotted in Figure 4.1 and details of the data are listed in appendix A.

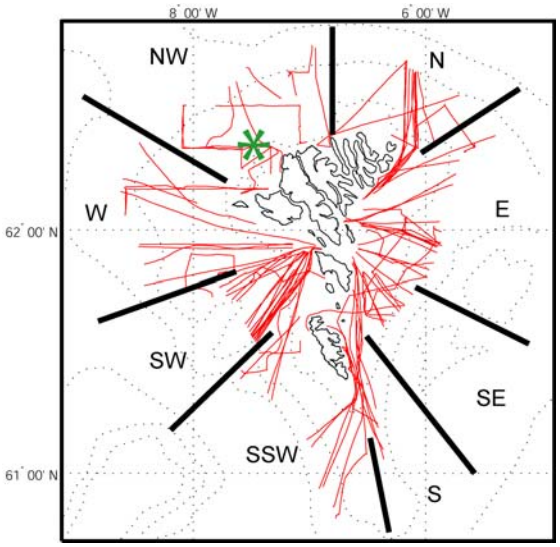

Figure 4.1. Track plot of 92 tracks on the Faroe Shelf. Thick lines are separation lines for direction groups. The letters are direction names. The green star in the NW direction is the position of Aanderaa Current Meter deployment 2985_010. The contour lines in this Figure are from GEBCO 95.

4.2 Quality control and calibration

The measured data have been quality controlled by a standard procedure based upon data variation with time in relation to neighbouring data values (spikes). The editing has been done partly automatically (excluding extreme values) and partly manually using an interactive graphical software package developed to edit these data. The software package is based upon MATLAB.

The SST data have been calibrated against CTD data. On cruises where CTD stations were operated, CTD stations showing a homogeneous surface layer, and where the SST at the same time showed a steady temperature, have been selected. For these stations, SST was plotted against CTD temperature from a shallow depth and this showed a linear relationship, y=ax+b. Figure 4.2 is an example of such a plot. For all the cruises the coefficient 'a' was constant within +/- 1%. The coefficient 'b' on the other hand was somewhat varying, but was fairly constant within each cruise. For cruises without CTD stations, the coefficient 'b' is interpolated linearly from the closest CTD cruises. The calibrated SST will typically have a standard error less than 0.05 °C.

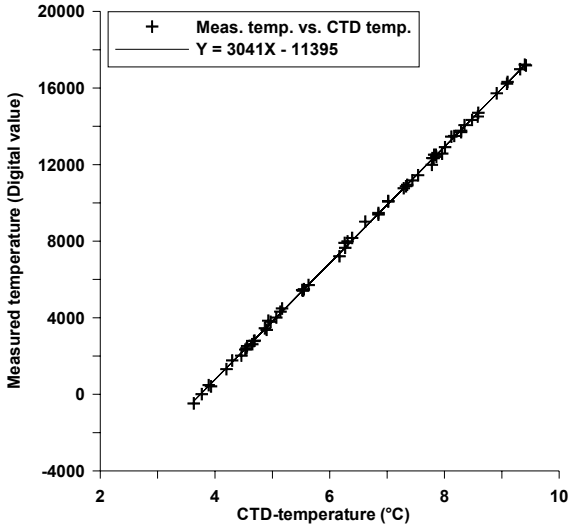

Figure 4.2. Calibration of measured SST (from approx. 3 m depth) vs. CTD surface temperature (from 3-5 m depth) on cruise 9932.

4.3 Exponential fit

For all tracks, the SST has been plotted against bottom depth. Many of these plots show a smooth or S- shaped step variation (Figures 4.3 and 4.4), with temperature increasing with depth. Therefore all plots have been fitted to two exponential functions:

$$F1(D) = A + B \times \exp[C(D - D0)] \text{ for } D \le D0 \quad (4.1a)$$

$$F2(D) = A + 2B - B \times \exp[-C(D - D0)] \text{ for } D > D0 \quad (4.1b)$$

A Fortran program has been written to make a "least square fit", finding the centre depth (D0) of the step and fitting depths shallower than D0 to function F1(D) (Eq. 4.1a) and depths larger than D0 to the function F2(D) (Eq. 4.1b). For some of the tracks, the program gave a good fit, but for others, the fit was poor because of, e.g. irregularities or short tails in the temperature/depth plot. Many of the fittings have thus been adjusted manually. Figure 4.3 is an example of an exponential fit of the SST, showing the functions F1(D) and F2(D).

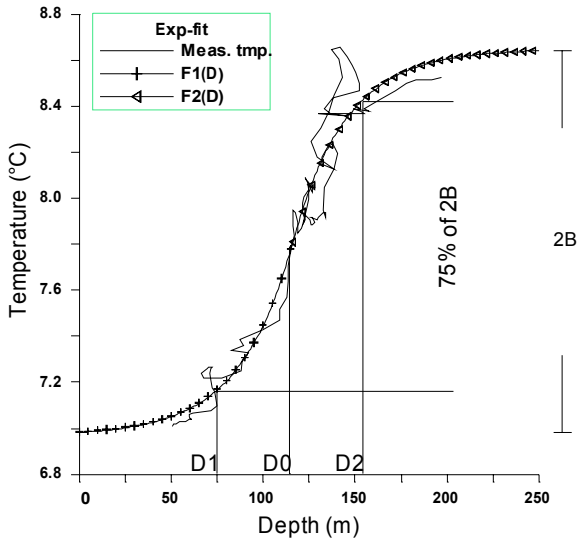

Figure 4.3. SST vs. bottom depth and exponential fit of the plot. D0 is centre depth of the front; D1 and D2 are inner and outer depth at the mid 75% temperature increase of the exponential fit (100%=2B).

4.4 Classification

For further analysis the data have been sorted by data quality and by geographic location. Regarding data quality, the tracks are grouped into four groups, where each group has specific demands on the data quality, i.e. the straightness of the track, and the regularity of the temperature change vs. depth. The groups are listed in Table 4.1 with specification and number of tracks in each group. Figure 4.4 shows an example of a SST vs. bottom depth plot for each of the four groups.

Table 4.1. The table lists group identity, specification for each group and number of tracks in each group.

Group	Specification	No. of tracks in group
I	1. Track is a straight line 2. Depth is continuously increasing/decreasing 3. Temperature is continuously increasing/decreasing	15
II	1. Track is a straight line 2. SST vs. bottom depth plot can have small irregularities 3. Fit of exponential function can be used to estimate the mid-depth and the width of the front.	27
III	1. Track can have small fluctuations 2. SST vs. bottom depth plot can have irregularities 3. Fit of exponential function can be used to estimate the mid-depth of front.	16
IV	1. Track can have fluctuations 2. SST vs. bottom depth plot can have large irregularities 3. Can not be fitted with an exponential function	34

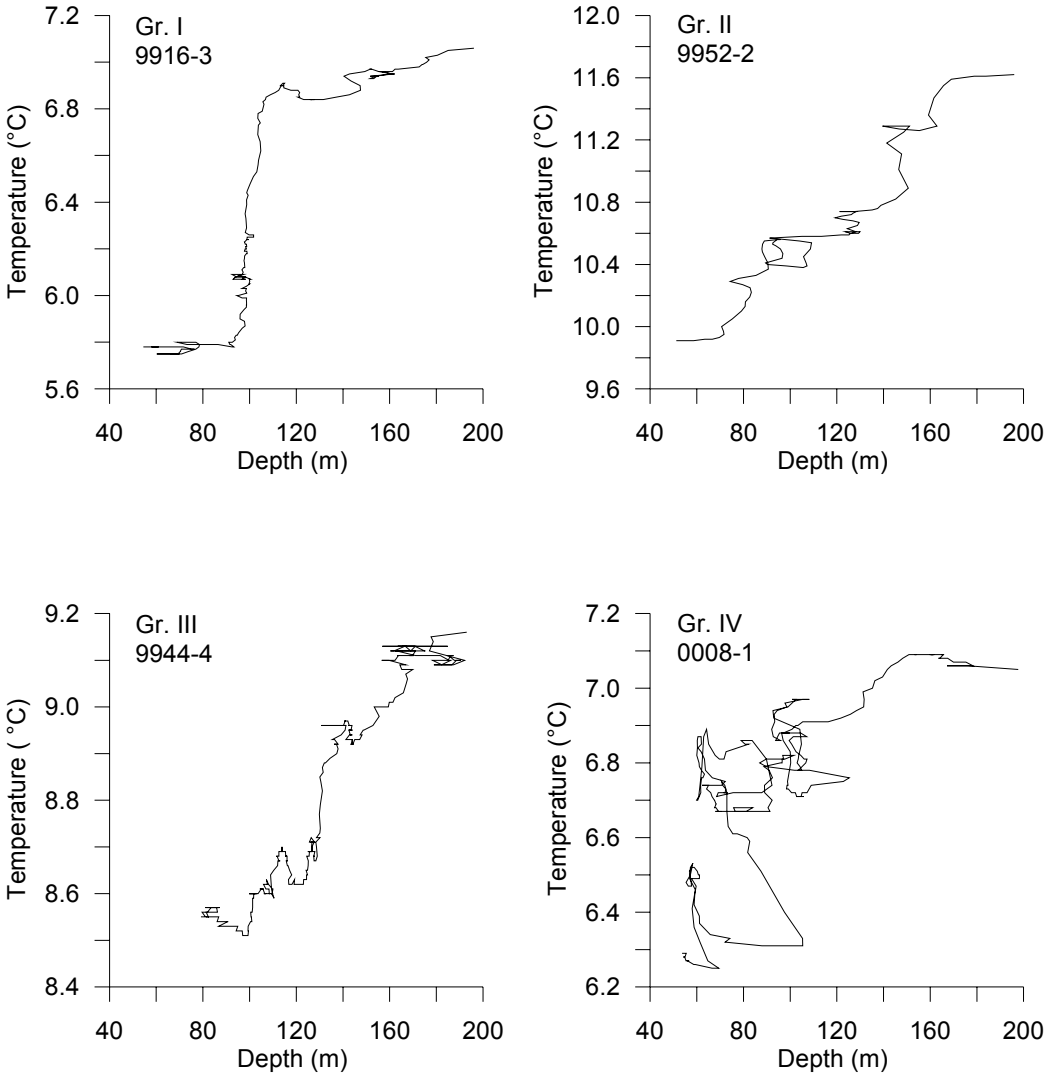

Figure 4.4. Examples of SST vs. bottom-depth plot from group I, II, III and IV, respectively. The tracks are randomly chosen within each group.

The tracks have also been grouped into eight geographic groups according to track direction from the shelf area and the topography of the shelf. For example, north of the Faroes, the shelf is wide and slowly deepening and covers several track directions. Therefore, directions with only few tracks are grouped together with neighbouring directions, if the topography is similar. Figure 4.1 shows all the tracks covered in this work with lines and letters showing the different geographic groups.

5 Results of SST data

5.1 Temperature change across the front

The on-shelf water temperature is almost always lower than the off-shelf water temperature. Only five of the 92 crossings of the front showed warmer water on the shelf (Appendix A). These five observations were from the months September, October and November and they all had a temperature difference lower than half a degree C. The data from all the 92 crossings show that the temperature difference between absolute maximum and absolute minimum along the track varies from -0.48 to 2.16 °C, where the minus sign indicates that the water is warmer on the shelf (Appendix A). In Figure 5.1, numbers of observations of temperature differences greater than 1.0 °C and lower than 0.5 °C, respectively, are plotted against the month of observation. The figure shows, that temperature differences greater than 1.0 °C most often occur from March to June, while temperature differences less than 0.5 °C are most common from September to February.

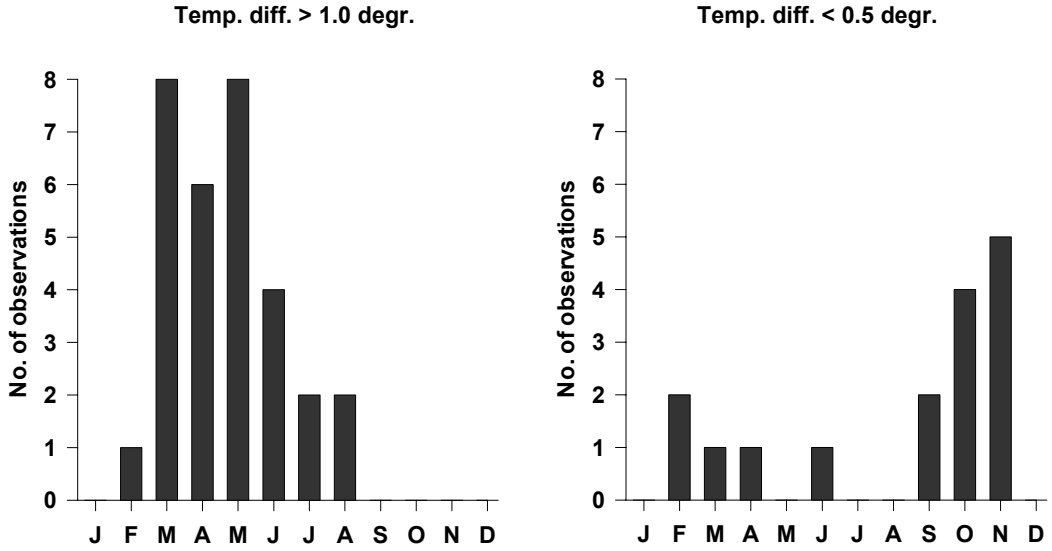

Figure 5.1 The left plot shows number of observations vs. month, where the cross frontal temperature difference exceeded 1.0 °C. Only crossings of type I, II and III in Table 4.1 are included. The right plot shows number of observations vs. month, where the temperature difference was less than 0.5 °C. Here most observations are of type IV, and only one, which did not have a straight track, was excluded.

From the exponential fit (Eq. 4.1), the B coefficient multiplied by two is an estimate for the temperature difference across the front (Figure 4.3). A plot of 2B against month should thus show the same pattern as in Figure 5.1. This is plotted in Figure 5.2 for all tracks in group I and II. As above, it is found that the largest differences occur from early spring to summer and are not found in the winter season, while small differences are most common from late summer and can occur until next spring.

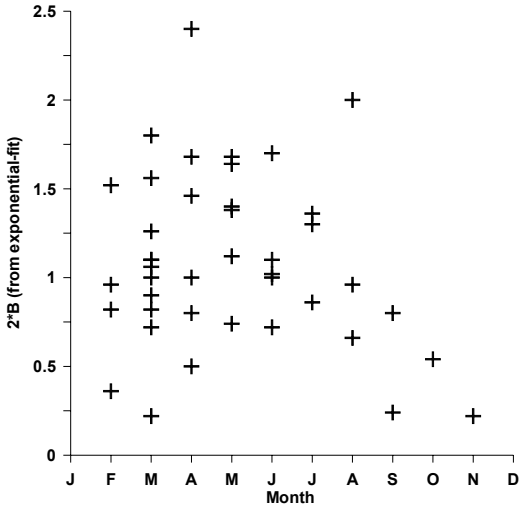

Figure 5.2. 2B coefficient from exponential fit (Eq. 4.1) vs. month of observation. All tracks (42) in group I and II are included.

5.2 Location and width of the front

For seven directions the mean D0 depth, which is the centre depth of the front estimated from the exponential fit, is calculated for all tracks in group I, II and III (direction S is excluded, because it has too few tracks in these groups). As an indication of the width of the front, the depths corresponding to the middle 75% of the exponential fit, shown as D1 and D2 in Figure 4.3, were found. For this estimation, only tracks in groups I and II are included, because in these groups, the temperature profile is estimated to be good enough to also fit the 'tails' of the exponential functions. Table 5.1 lists the mean of D0, D1 and D2 for each of the seven directions.

Table 5.1. The table lists for seven directions (Fig. 4.1) the calculated mean for depths D0, D1 and D2 and their respective standard error. For D0 all tracks in group I, II and III are used, while only tracks from group I and II are used for calculation of the mean of D1 and D2. Also listed are the difference between D1 and D2 and the number of tracks included in the calculations of D0, D1, and D2.

Direc-tion	Mean D0 (m)	Std. Err. for D0	Mean D1 (m)	Std. Err for D1	Mean D2 (m)	Std. Err for D2	D2-D1	No. of tr. D0	No. of tr. D1, D2
E	105	5	72	6	140	7	68	13	10
SE	87	3	62	6	105	6	43	8	6
N	114	6	82	6	150	11	68	8	6
NW	104	4	91	2	112	1	21	6	2
SW	141	6	113	13	170	8	57	10	8
SSW	163	6	154	8	189	6	35	6	4
W	153	8	119	9	170	9	51	5	4

The values in Table 5.1 show, that the centre depth, D0, is much deeper for the three directions west, southwest and south southwest than for any other direction.

In Table 5.1 is also listed the vertical extent of the front as D2-D1, i.e. the depth range, which the front is covering. The smallest depth range is found in the direction northwest, which also is the widest and flattest area of the shelf. The largest depth ranges are found in the north and east directions, and these directions have the most continuously increasing bottom depth without large steps in the topography, that is covered by the tracks.

5.3 Neap-spring frontal movement

The tidal front theories presented in Chapter 3 are dependent on the mean tidal velocity. Since the magnitude of the tidal velocity may change significantly in a fortnightly period, it may be expected that the front changes its position during this period. It is thus to be expected that the front advances off-shelf during increasing tidal velocities and retreats during decreasing tidal velocities. That is, the frontal mean depth is expected to be dependent on the tidal velocity or the tidal velocity averaged over a few days before the observation.

To investigate the possibility of such a frontal movement with the neap-spring cycle (Lunar fortnightly), normalised depth anomalies from 56 tracks from the groups I, II and III have been plotted in Figure 5.3 against the cube of the velocity averaged over the last seven days before the track event (including the day of the track event). Since the mean depth is varying for each direction, the depth is normalised according to its direction. The velocity is a prediction calculated from an Aanderaa Current Meter time series – deployment 2985_010 (Hansen & Larsen, 1999) at a position north westerly on the Faroe Shelf (Fig. 4.1). Bottom depth is 98 m and instrument depth is 40 m, while the length of the time series is about 6½ months. The correlation coefficient for the values in Figure 5.3 was only -0.0005, and thus not significant. Tests were also made averaging from one up to six days before the track event (not shown), but these did not show any correlation either.

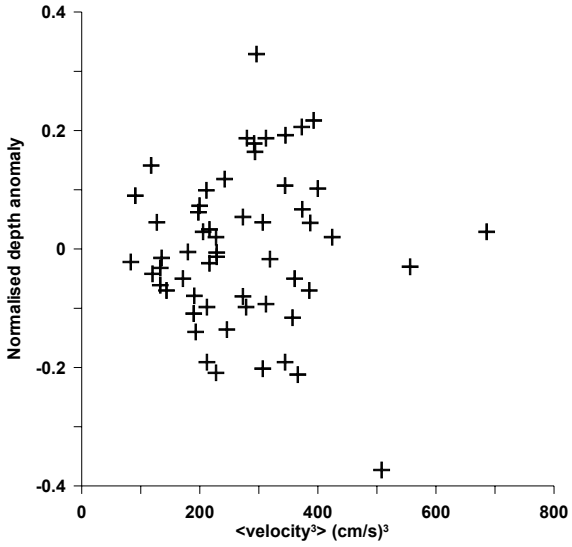

Figure 5.3. Normalised depth anomaly vs. the cube of predicted velocity averaged over seven days. The predicted velocity is first calculated every 12 minutes. These values are cubed. Then the average for the day of the track and six days before the track is calculated. For normalising the depth, the mean depth in each direction is calculated. The normalised depth anomaly is then the actual depth minus mean depth divided by the mean depth for the actual direction. All tracks (56) from group I, II and III are included, except two from direction South, which are not included in the estimation of D0 (Table 5.1).

The same procedure has been made on 41 tracks from the months March, April, May and June, which are the months, when large temperature differences across the front most often are observed (Fig. 5.1). The depths have been re-normalised to include these 41 tracks only, and are again normalised according to their direction. These results are plotted in Figure 5.4. The correlation coefficient for this plot is 0.09, so there is again no significant correlation.

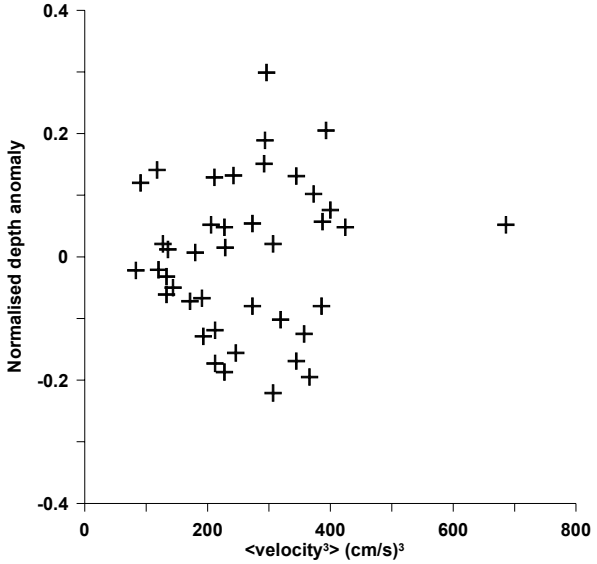

Figure 5.4. 41 tracks from group I, II and III in the months March, April, May and June are included. For explanation of calculating the averaged velocity and normalised depth anomaly, see text for Figure 5.3.

5.4 Seasonal variation

Since a seasonal variation is observed in the cross frontal temperature difference (Fig. 5.1), a seasonal dependence of the location of the front could be possible. This is tested in a similar manner as in the previous section, by plotting normalised depth anomaly vs. month of observation (Fig. 5.5). The same 56 tracks as in Figure 5.3 are used for the test.

A possible seasonal variation could be tested by fitting a sinus curve to the observations. But since the normalised depth range is large for the well represented months and the months from July to November are poorly represented, this could have produced an artificial result. I therefore conclude on the basis of Figure 5.5, that my data do not show any significant seasonal variation in the location of the front

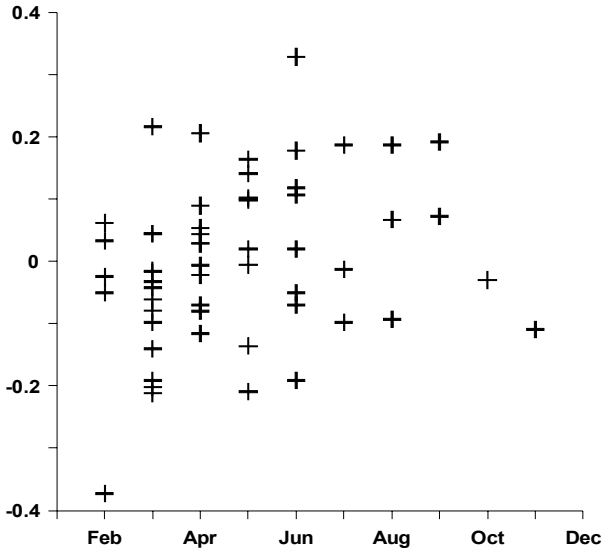

Figure 5.5. Same tracks as in Figure 5.3, showing normalised depth anomaly vs. month of observation.

6 Heat Budget

The SST measurements show, that the temperature on the shelf is almost always lower than off the shelf. The reason for this might be found in the heat budget of the shelf and its surroundings. On the shelf we find, that the water mainly flows along constant depth contours and thus remains at approximately the same depth for a long time. Since the heat flux through the surface averaged over a year is negative, the water on the shallow parts of the shelf most of the year will be cooler than the deeper parts, because the shallow parts have a smaller water mass to cool. In the summer, the shelf water will, of course, also be more effectively heated than the off-shelf water, but the stratification of the off-shelf water diminishes this effect. To balance the cooling through the surface, the shelf water will need a net gain in heat flux from its surrounding water masses.

A heat budget for the Faroe Plateau and surroundings is calculated to determine if it can explain the fact that on a monthly mean basis, the front is most pronounced in February and March (Fig. 2.6).

6.1 Calculations

The seasonal heat balance of the Faroe Shelf is calculated using a monthly mean net air-sea heat flux from Lindau (2001) and the bottom topography matrix from the tidal model (Appendix B).

A simple model is used, in which the topography of the Faroe Shelf is smooth and circular with increasing depth from the islands to off-shelf. If depth contours starting at 80 m depth are drawn and extending off-shelf to 150 m depth with 10 m interval (Fig. 6.1) we get annular blocks, where the inner and outer sides of each block follow two different bottom contours. The innermost block is filled with land in the middle, but otherwise represents the shelf water from 0 to 80 m bottom depth. The block representing the off-shelf water column is taken from the 150 m bottom contour and extending horizontally to the border of the depth matrix, except for areas shallower than 500 m (e.g. the Scottish Shelf) and extending vertically from the surface to the bottom depth, though at a maximum down to 500 m, which is taken as the depth limit for convective mixing (Hansen and Østerhus, 2000). In between the on-shelf and off-shelf blocks, we have the “transition” blocks representing the frontal area. Each block is considered as homogeneous and to make the calculations simple, a heat gain or loss is immediately distributed throughout the water column, thus ignoring a possible surface stratification. Heat fluxes are allowed through the surface and the sides of the water blocks only.

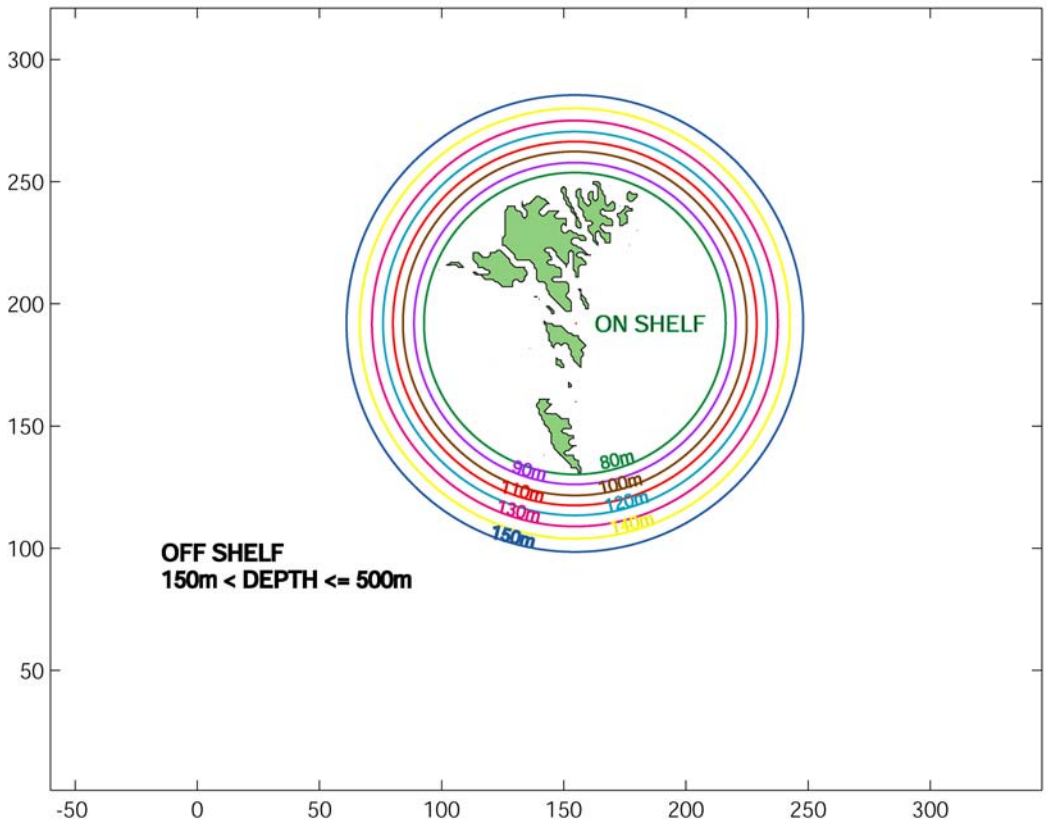

Figure 6.1. Rough outline of assumed depth contours used in calculating the heat budget.

The calculations are done in a Matlab script file. For each block, all the grid points in the depth matrix with depth values within the block's depth interval are counted and used to calculate the surface area and volume for the block. The surface area (A_i^{surf}) and volume (V_i) for the i'th block then are:

$$A_i^{surf} = N_i A_{grid}\,, \qquad V_i = A_{grid} \sum_{j=1}^{N_i} D_j^i \qquad (6.1)$$

where N_i is the number of grid points inside the i'th block, A_{grid} is the area of one grid cell, and D^i_j is the bottom depth at the j'th grid belonging to the i'th block. The surface area is then used to calculate the circumference (C_i) and hence the area of the side (A_i^{side}) of each assumed annular block described above:

$$C_i = 2\sqrt{\pi \sum_{j=0}^{j=i} A_j^{surf}}\,, \qquad A_i^{side} = H_i^{outer} C_i \qquad (6.2)$$

where H_i^{outer} is the outer depth of the i'th block and A_0^{surf} represents the land area. The circumference and the area of the side for instance for the shelf water block then becomes: $C_1=2(\pi\ (A_0^{surf} + A_1^{surf}))^{½}$ and $A_1^{side} = 80\ C_1$, respectively. The calculated values are listed in Table 6.1. Using these calculations, the surface area and the volume of each block are fairly realistic, while the area of the sides will be somewhat underestimated, since the bottom contours in reality are not circular.

Table 6.1. The table lists calculated areas, etc. from the topography matrix. The first column lists the index *i*, with a description of the corresponding annular block in parenthesis. The second and third column list the surface area and volume of each block, respectively, while the fourth column lists the volume accumulated. The fifth column lists the surface of the outer side as calculated by Eq. (6.2) (right), and finally the sixth and seventh columns list the circumference and radius of the annular blocks, evaluated at the outer side.

i (block)	A_i^{surf} (km^2)	V_i (km^3)	V_i acc (km^3)	A_i^{side} (km^2)	C_i (km)	R_i (km)
0 (0 m)	1514	0.0	0.0	0.00	138.0	21.96
1 (80 m)	2953	180.0	180.0	18.96	236.9	37.71
2 (90 m)	988	83.7	263.7	23.57	261.9	41.67
3 (100 m)	1254	120.2	383.9	29.04	290.4	46.22
4 (110 m)	1705	179.0	562.9	35.77	325.2	51.76
5 (120 m)	1348	154.7	717.6	42.03	350.3	55.75
6 (130 m)	1252	156.8	874.4	48.37	372.1	59.22
7 (140 m)	1218	164.3	1038.7	54.90	392.1	62.41
8 (150 m)	1079	156.5	1195.2	61.36	409.1	65.10
9 (>150 m)	50313	24261.0	25456.2			

The calculations start in October, where we assume, that all the water columns have equal temperature. This is based on temperature measurements on-shelf and off-shelf, which show, that these temperatures are almost equal in October and that the off-shelf water column at that time is approximately homogeneous (Fig. 2.6). The calculations run for a year in time steps of one day, where the net air-sea heat flux is assumed constant within each month. The heat flux through the sides is assumed proportional to the temperature difference between adjacent columns with a proportionality constant k, which is assumed equal for all columns. The total heat diffusion is calculated at each time step and the temperature change of the i'th column at each time step then is:

$$\Delta T_i = \frac{\Delta t}{C_p \rho V_i}\left[QA_i^{surf} - kA_{i-1}^{side}(T_{i-1} - T_i) + kA_i^{side}(T_i - T_{i+1})\right] \qquad (6.3)$$

where Δt (s) is the time step, C_p (J Kg^{-1} $°C^{-1}$) is the specific heat of seawater, ρ (Kg m^{-3}) is the density of seawater, Q (W m^{-2}) is the net air-sea heat flux, T_i (°C) is the temperature of the i'th water column and k (W m^{-2} $°C^{-1}$) is the proportionality constant introduced above. For the innermost water column (i = 1) the area A_0^{side} is zero, since H_0^{outer} is zero. For the off-shelf water column, T_{i+1} is not defined. Instead a constant heat input, Q_{in} (W), is supplied to balance the net heat loss through the surface of all the columns. The temperature change of the off-shelf column then is:

$$\Delta T_i = \frac{\Delta t}{C_p \rho V_i}\left[QA_i^{surf} - kA_{i-1}^{side}(T_{i-1} - T_i) + Q_{in}\right] \qquad (6.4)$$

This added heat input can be regarded as representing the heat input from the North Atlantic Current and is assumed constant.

6.2 Results

The model was run several times with different values of k and Q_{in}, aiming to find the result, which best fitted the observed monthly mean temperature variations on-shelf

and off-shelf as given in Figure 2.6. The on-shelf temperature and the off-shelf temperature at 100 m depth from Figure 2.6 are reprinted in Figure 6.2.

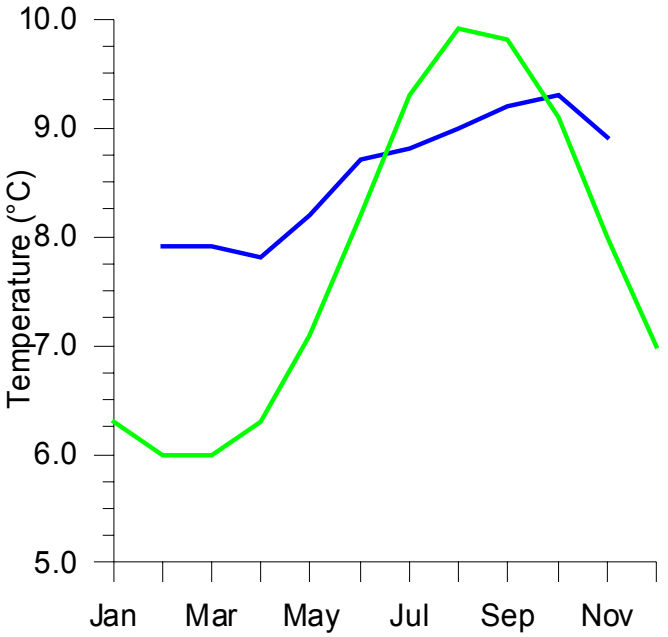

Figure 6.2. Same plot as in Figure 2.6, showing monthly mean temperatures on-shelf (green) and off-shelf (blue), where the off-shelf temperature is represented by the monthly mean temperature in the Faroe Bank Channel at 100 m depth.

The best fit gave a value of k equal to 70000 W m^{-2} °C^{-1}. To compare k with the horizontal kinematic eddy diffusivity K_H we note, that the heat flux by turbulent diffusion J is given by (Pond and Pickard, 1986):

$$J = C_p \rho K_H \frac{\partial T}{\partial x} \cong C_p \rho K_H \frac{\Delta T}{\Delta X} \qquad (6.5)$$

where ΔT is the temperature difference between two adjacent columns and ΔX is an expression for the average distance, which is approximately the column width. Since the heat flux through the sides of the columns is represented by $k\Delta T$ (Eq. 6.3) this implies that

$$C_p \rho K_H \frac{\Delta T}{\Delta X} = k\Delta T \Leftrightarrow K_H = \frac{k\Delta X}{C_p \rho} \qquad (6.6)$$

Using $C_p = 4.0 \cdot 10^3$ J Kg^{-1} °C^{-1} (Loder and Greenberg, 1986), $\rho = 1028$ Kg m^{-3}, $\Delta X =$ 3913 m, which is the mean width of the annular blocks, and using the value of k given above, this results in K_H = 67 m^2 s^{-1}. According to Pond and Pickard (1986), the range of values for K_H are similar to those for the eddy viscosity A_H which are between 10 and 10^5 m^2 s^{-1}. This means that our estimation of the eddy diffusivity is in the lower end of the range.

Increasing or decreasing the value of k with only 5000 W m^{-2} °C^{-1} resulted in an appreciably poorer fit of the on-shelf temperature variation to the measured mean

temperature variation. These changes in the value of k had only small effects on the fit of off-shelf temperature variation.

The constant heat input, Q_{in}, was adjusted to achieve approximately the same temperature on-shelf at the end of the calculations as when the calculations were initiated. The chosen value for Q_{in} equals 4.2 TW. Most of this heat probably originates from the Faroe Current, which is a branch of the North Atlantic Current. This heat input to the Faroe Shelf thus corresponds to a temperature decrease of the North Atlantic water passing the Faroes. This temperature decrease can be estimated as Q_{in} divided by ρ, C_p and the volume flux of Atlantic water crossing the Iceland-Faroe ridge. Using the latest estimate of the Atlantic water volume flux equal to 3.5 Sv (Hansen *et. al.*, 2003) the temperature decrease is approximately 0.3 °C.

The model results of the seasonal temperature variations are plotted in Figure 6.3, where the extreme curves can be considered as representing the on-shelf water (green curve, 80 m) and the off-shelf water (black curve, >150 m). It is seen (Fig. 6.3), that the largest temperature differences are found in January, February and March, and that the on-shelf water is warmer than the off-shelf water in July, August and September, though having in mind, that we have neglected the off-shelf stratification. The same characteristics can be found in Fig. 6.2, comparing the measured monthly mean on-shelf and off-shelf temperature variations. Consequently, the heat budget explains the pronounced front observed in late winter/early spring.

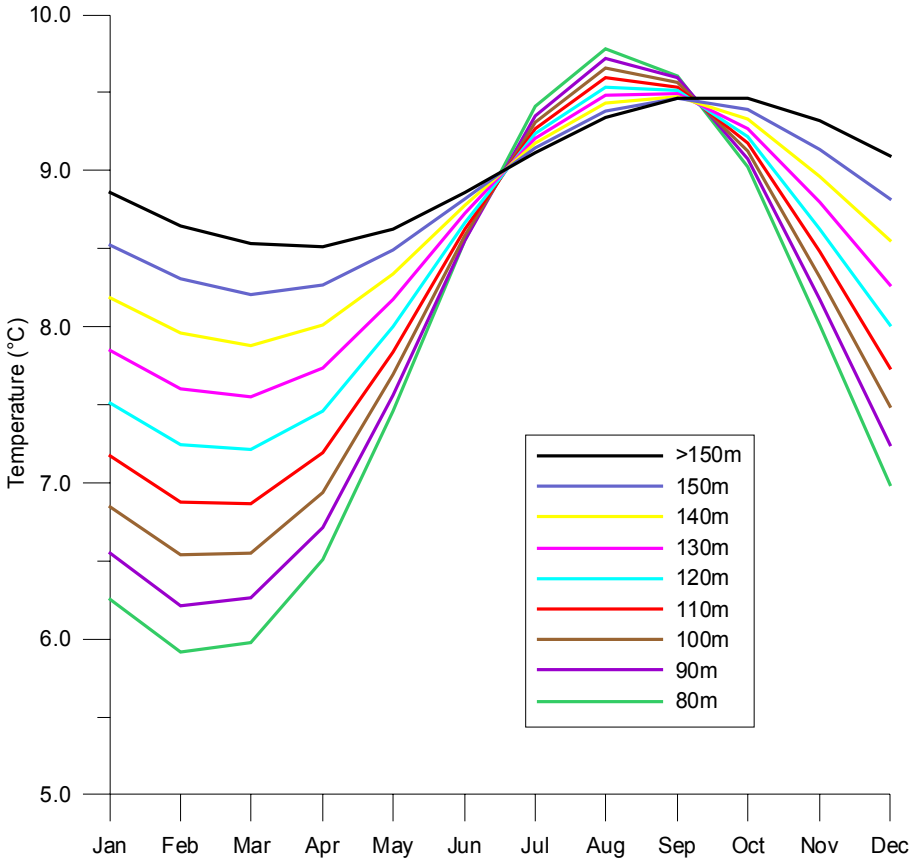

Figure 6.3 Heat balance through the year calculated for 9 assumed water columns.

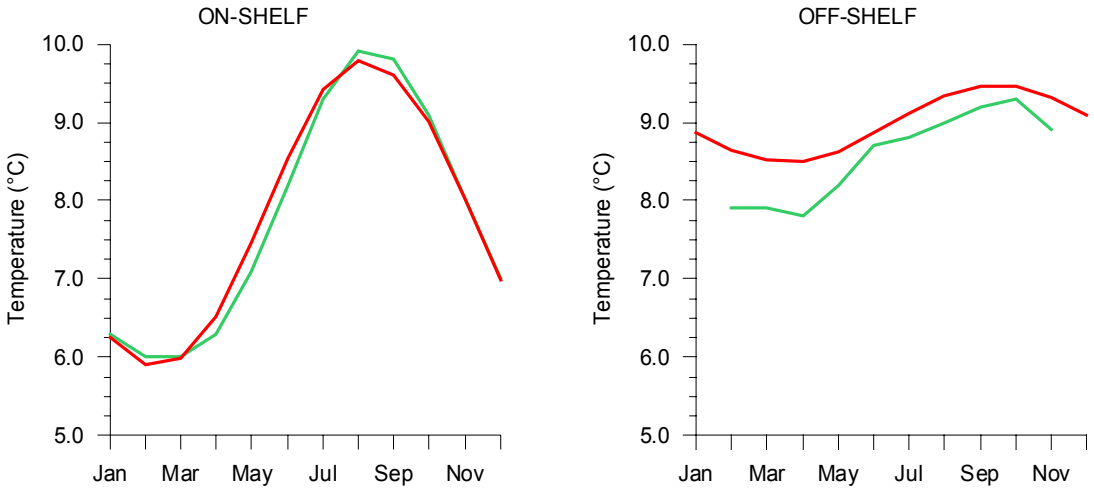

Figure 6.4. The result from the Heat Budget (red) compared to monthly mean temperature (green) from Figure 6.2. The left plot shows seasonal temperature variation on-shelf, while the right plot shows the off-shelf variation.

In Figure 6.4, left plot, the curve representing 80 m from the calculations (Fig. 6.3 green) is plotted together with the monthly mean temperature on-shelf from Figure 6.2. To the right are plotted the greater than 150 m curve (Fig. 6.3 black) and the monthly mean temperature off-shelf (Fig. 6.2). It is seen, that the calculated heat balance reproduces the seasonal temperature variation to a reasonable degree, especially on-shelf. Off-shelf, there is a temperature offset in the heat budget, and also, the seasonal amplitude is smaller than in the observations.

7 Comparison of observations and theories

In this chapter the location of the tidal front is predicted by the tidal theories described in Chapter 3.1 and 3.2 and compared to the observed location of the front. In predicting the tidal front, velocity data are used from the tidal simulation model by Simonsen (1999), described in Appendix B. Depth mean M_2 amplitude averaged over a tidal period is applied, since this is generally accepted in similar work (Simpson, 1998). Finally, the possibility of the Faroe Shelf Front being a shelf-break front is discussed.

7.1 H/U^3

In this section the H/U^3 theory based on a positive surface heat flux is tested. Since the net heat flux at the Faroe Islands is positive only from May to August (Lindau, 2001), this theory can only predict the position of the front in these months. The prediction of the front is given by Equation 3.8. In the term on the right hand side of the equation the following constants are used: $C_p=4.0\cdot10^3$ J Kg^{-1} $°C^{-1}$, g=9.81 m s^{-2}, $\alpha=1.6\cdot10^{-4}$ $°C^{-1}$. (from Loder and Greenberg, 1986) and $\varepsilon_t=4.0\cdot10^{-3}$ (from Simpson, 1998). Adjusting Q to the local area to a value between 40 and 100 Wm^{-2} in the summer season (Lindau, 2001), we find that H/D_t (in SI-units) should equal 510 and 204 for the two values of Q, or that log10 (H/D_t) should equal 2.7 and 2.3, respectively. Figure 7.1 is a plot of log (H/D_t) at constant values 2.3 and 2.7, where H is the depth matrix from the tidal simulation and D_t is calculated using the M_2 velocity cubed (as described in Appendix B) and using $\rho=1028$ Kg m^{-3} and $C_d=0.0026$.

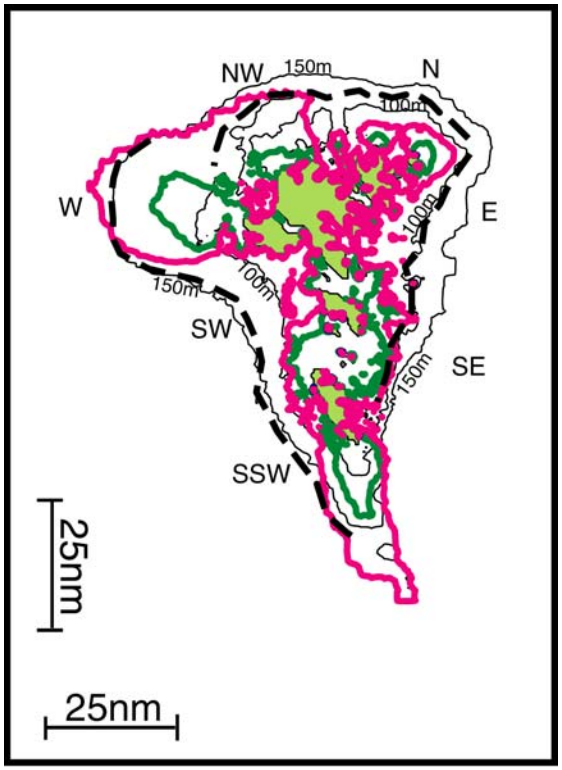

Figure 7.1: Part of model domain (Simonsen, 1999) with 100 and 150 m bottom contours. Also plotted are the log (H/D_t) contours at 2.3 (green) and 2.7 (magenta), where H is the tidal model bottom topography and D_t is calculated using the M_2 velocity cubed from the tidal model (Appendix B). The dashed black curve is the result from the SST measurements and shows the mean location of the front grouped in directions (see Table 5.1).

It is seen in Figure 7.1, that the curve representing Q = 40 W/m^2 is only in the northwest corner similar to the measurements, while the remainder of that curve as well as the curve representing Q = 100 W/m^2 predicts the front to be at a shallower location. The dashed curve in Figure 7.1 indicating the observed frontal location, is based on all tracks in group I, II and III and thus includes observations from all months. However there are no indications in the data, that the location of the observed front has a significant seasonal variation (Fig. 5.5).

7.2 H/U

The next theory to be tested is the bottom Ekman Layer, where the prediction of the front is given by Equation 3.9. Loder and Greenberg (1986) and Stigebrandt (1988) find good agreement in the Gulf of Maine and the Irish Sea, respectively, using λ=0.2. Loder and Greenberg (1986) imply, that λ is usually in the range 0.1 to 0.4, and the result for four values in this range is plotted in Figure 7.2, where again the velocity is drawn from the tidal model (Appendix B), C_d=0.0026 and the local Coriolis parameter f=1.28·10^{-4} s^{-1}.

It is seen (Fig. 7.2), that all the curves are within the 100 m bottom contour and do not fit the observations drawn as dashed lines in Figure 7.1. This theory thus predicts the front at a far too shallow location.

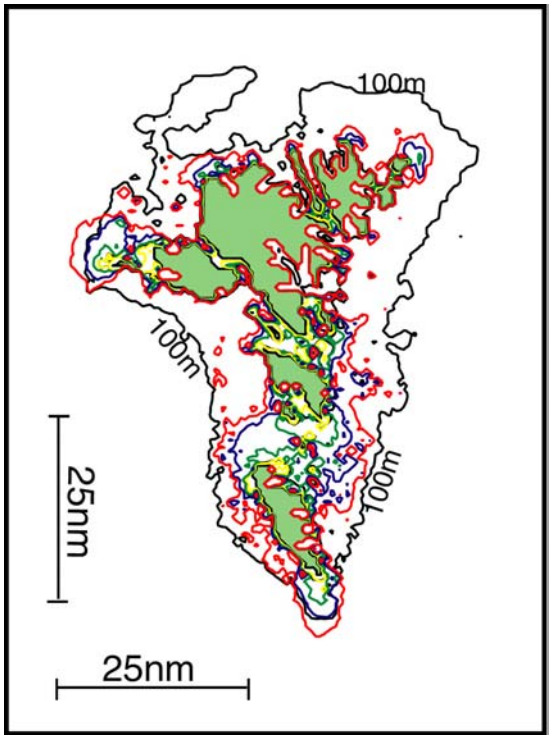

Figure 7.2. Contours of H/U = $\lambda(C_d)^{½}$/f. C_d=0.0026, f=1.28·10^{-4}, λ=0.1(yellow), 0.2(green), 0.3(blue) and 0.4(red).

7.3 H/U including rotation of the tidal ellipse

The last tidal theory to be tested is by Soulsby (1983) and includes the rotation of the tidal ellipses. By this theory, the thickness of the mixed layer is given by Equation 3.13. A plot of $H/\delta = 1$, thus predicts the location of the front. δ is calculated using C=0.075 (Soulsby, 1983) and the M_2 tidal semi-axis from the tidal model (Simonsen, 1999). C_d and f have the same values as given in the previous section and $\omega = 1.4 \cdot 10^{-4}$ s^{-1}.

It is seen in Figure 7.3 that the prediction of the frontal location of the H/U theory with inclusion of the rotation of the tidal ellipses fits fairly well to the observed location of the front except for the southwest and south-southwest directions.

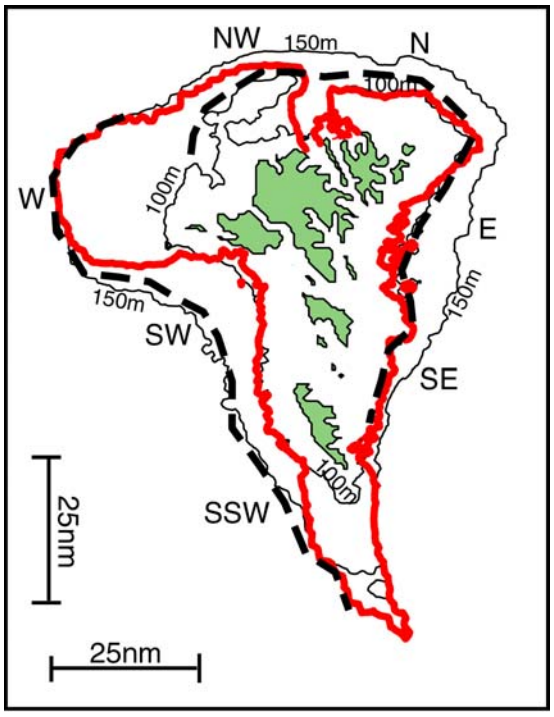

Figure 7.3. Contour of $H/\delta = 1$ (red), where δ is as defined in Eq. 3.13. Dashed curve shows observed frontal location.

7.4 Shelf-break front

As described in section 3.3, a shelf-break front can be found at or close to the shelf break. The task here is therefore to locate the shelf break on the Faroe Plateau and compare it to the observed frontal location.

Figure 7.4 shows the bottom topography of the Faroe Plateau, and it is seen, that the area within the 200 m contour is relative level. From the 200 – 300 m contour the bottom becomes steeper, and these contours can therefore be considered to represent the shelf break. The Plateau is approximately shaped as a triangle, and at the eastern side the 300 or 350 m contour represents the shelf break. At the northern and western sides, the bottom is getting steeper from approx. the 200 m contour, which therefore represents the shelf break there.

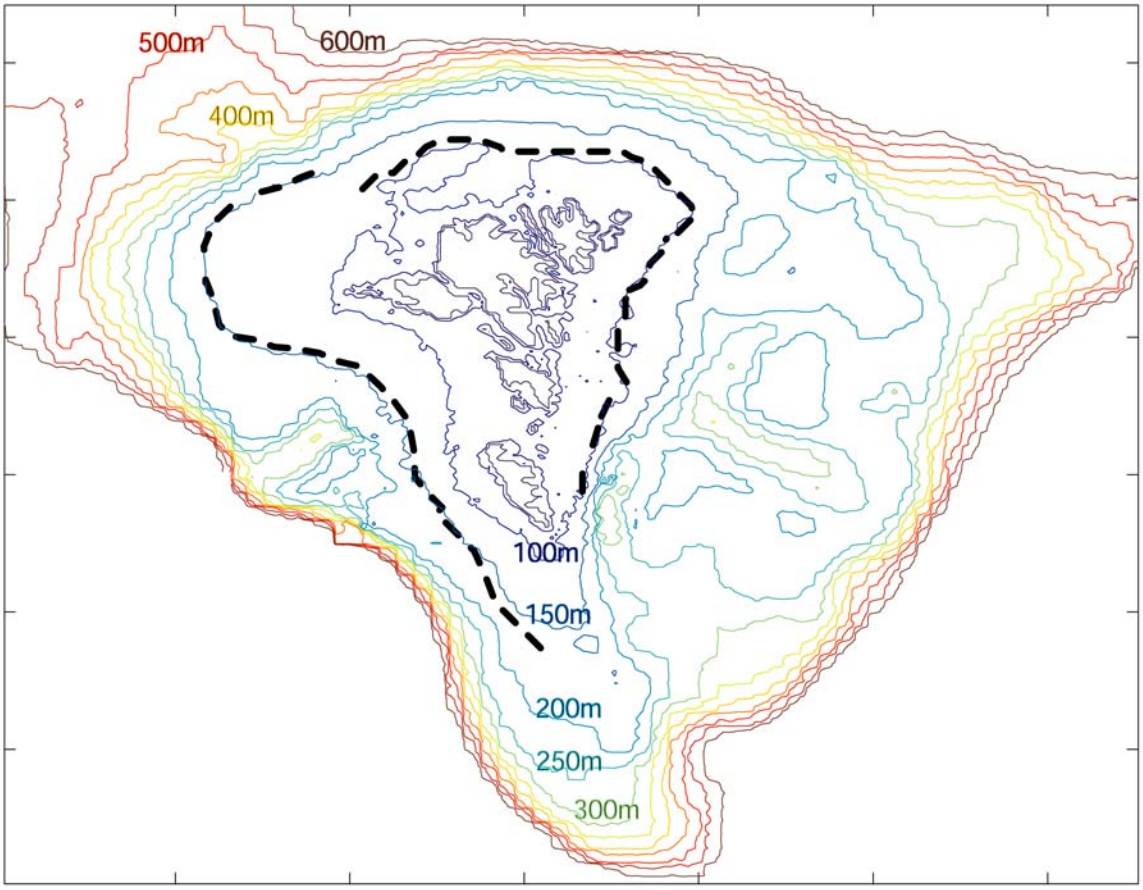

Figure 7.4. Depth contours from 0 to 600 m with 50 m interval of the Faroe Plateau based on depth matrix from the tidal simulation (Appendix B). Observed mean location of the front (Table 5.1) is indicated by dashed black lines.

In figure 7.4 the observed mean frontal location is also sketched, and it is everywhere within the shelf break. On the eastern side of the shelf, the frontal location is more than 75 km from the shelf break, and the front can therefore not be considered as a shelf-break front. At the northern and western sides, the mean location of the front is 10-20 km from the shelf break, which is on the order of daily fluctuation (Larsen et. al, 2001). As mentioned above the observed location of the front is at the surface.

8 Discussion

The data used to analyse the Faroe Shelf Front are SST data from the R/V Magnus Heinason. These data are not collected for the purpose of analysing the front and are collected over all seasons of the year. Nonetheless there is no indication in the data, that there is a seasonal variation in the location of the front (Fig. 5.5). The data cover large areas of the Plateau and it is therefore possible to compare the front at several locations. Mavor and Bisagni (2001) used satellite-derived SST data to map the temperature front on Georges Bank. The advantage of satellite-derived SST is, that it is a two dimensional picture, while the SST data used in this thesis are one dimensional. But both the spatial and the temperature resolution is much better in the one dimensional SST data compared to the satellite-derived SST.

The temperature vs. depth plot of all the SST data in groups I, II and III have been fitted with an exponential function for the main purpose of estimating a centre depth D0 of the front. For the s-shaped SST tracks the method is fairly good, but depends on the length of the tails. Therefore, tracks in group I and II are reliably estimated, while tracks in group III give a poorer estimate. When starting to analyse the SST data, it was expected that the mean D0 depth would be approximately 100 m, and therefore only data between 50 m and 200 m were included. But in the western and south-southwestern parts of the shelf the mean D0 depth exceeds 150 m. This means, that at these locations, many of the tracks do not have much room for the off-shelf tail and this possibly results in an underestimate of the D0 depth.

In calculating the heat budget for the Faroe Shelf and its surroundings, attempts were made to fit both the on-shelf and off-shelf temperature variations perfectly at the same time, but without success. One reason for this probably is, that the off-shelf temperature is based on one standard CTD station only, which therefore might not represent the mean temperature of the whole off-shelf area. Other reasons might be the neglect of the off-shelf stratification, which in the summer months results in slightly greater temperatures. Finally Q_{in} might not be constant, but might have a seasonal variation. Indeed, Hansen *et. al.* (2003) find that the Atlantic water flux across the Iceland-Faroe ridge does not have a significant seasonal variation of volume flux, but that the temperature of the Atlantic water has a seasonal amplitude of 0.58 °C. This implies a seasonal variation in Q_{in}, which may be strengthened or weakened by a possible seasonal variation of the exchange rate between on-shelf and off-shelf waters.

A by-product of the heat flux model is an estimation of the horizontal kinematic eddy diffusivity K_H, which can be used to estimate the exchange rate of shelf water. The estimated value of K_H equals 67 m^2 s^{-1}. Compared to the result from a simple temperature model for the Georges Bank (Loder *et. al.*, 1982) this value is low, but in a

model of formation of a shelf/slope front (Chapman, 1986) a K_H equal to 100 m^2 s^{-1} is used.

The observed location of the front is compared to theories on tidal fronts, but the effect of the wind mixed layer is not included. The comparison reveals, that the H/U^3 theory in most areas predicts the Faroe Shelf Front at a too shallow location (Fig. 7.1). The H/U^3 theory is based on a positive heat flux in the summer season, and thus predicts the location of a summer front, which is established because of an off-shelf stratification advancing on-shelf during summer. In Figure 2.6 it may seem as if the seasonal thermocline off-shelf is well established, but measurements show, that this is only true for the month of July. In the other summer months, the seasonal thermocline is only transient (Hansen, 2000). This is in contrast to, for example the Georges Bank, where off-shelf stratification advances on-shelf and thus establishes a seasonal front (Mavor and Bisagni, 2001). Also, as previously mentioned, there is no indication of a seasonal variation in the location of the front, and therefore this theory can not be expected to predict the frontal location.

In comparing the H/U theory with the observations, it is found that a bottom Ekman layer, as used by Loder and Greenberg (1986) and Stigebrandt (1988), can not explain the location of the front (Fig. 7.2). This theory only includes the effect of the rotation of the earth and presumably is too simple. An improvement of this theory is the H/U theory including the rotation of the tidal ellipse (Soulsby, 1983). This theory predicts the observed location of the front fairly well except in the directions towards southwest and south-southwest, where frontal depths are somewhat underestimated (Fig. 7.3). One reason for this might be that the M_2 velocity in the tidal model is slightly underestimated (Simonsen, 1999). Another reason might be, that the H/U theory, discussed here, is not the whole story. As previously mentioned, the surface Ekman layer is ignored and this might not be a good assumption for the Faroese region, which is generally considered as windy (Cappelen and Laursen, 1998).

The observations of the front show that the front is at deeper locations in the directions towards the west, southwest and south-southwest (Table 5.1). Simpson (1998) points out, that in the H/U theory including the rotation of the ellipses, not only the strength of the tide, but also the polarisation of the tidal ellipse controls the position of the front (Eq. 3.12). It is seen in Figure 8.1, that the polarisation of the M_2 tide increases numerically towards the off-shelf water, especially west of the Faroes and in the southwest direction and thus fits the pattern of the observed mean depth of the front (Table 5.1). Comparing Figure 7.1 and 7.3 it is seen, that the Soulsby (1983) theory is better at predicting the frontal location towards the southwest and south-southwest directions, but not sufficiently.

This lack of the Soulsby (1983) theory can be explained by assuming, that the front is at the location, where the surface mixed layer plus the bottom mixed layer equal the bottom depth, and that the surface mixed layer has an asymmetry with larger depths in the south westerly directions, since the most frequent wind direction in the area is from southwest (Cappelen and Laursen, 1998). This could give a better fit to the observations. Another explanation might be found in the tendency of the flow to follow isobaths. The mean flow

around the islands is anticyclonic, implying that the deep location of the front south of the islands is advected north wards west of the islands. The mean D0 depth is decreasing from direction south-southwest to direction southwest, but because of the tendency of the flow to follow isobaths, the distance travelled is perhaps too short for the front to adjust to the new environment.

Regarding proximity to the shelf break, the observed surface location of the front is relatively close to the shelf break at the western and northern sides of the Faroes, but not at the eastern side. From the SST data it is not possible to investigate if the foot of the front is associated with the shelf break. To clarify this, further investigations are necessary, which resolve temperature and salinity distribution with depth. The existing standard CTD sections from the shelf and off shore are not sufficient for this purpose, since the station spacing is 10 km.

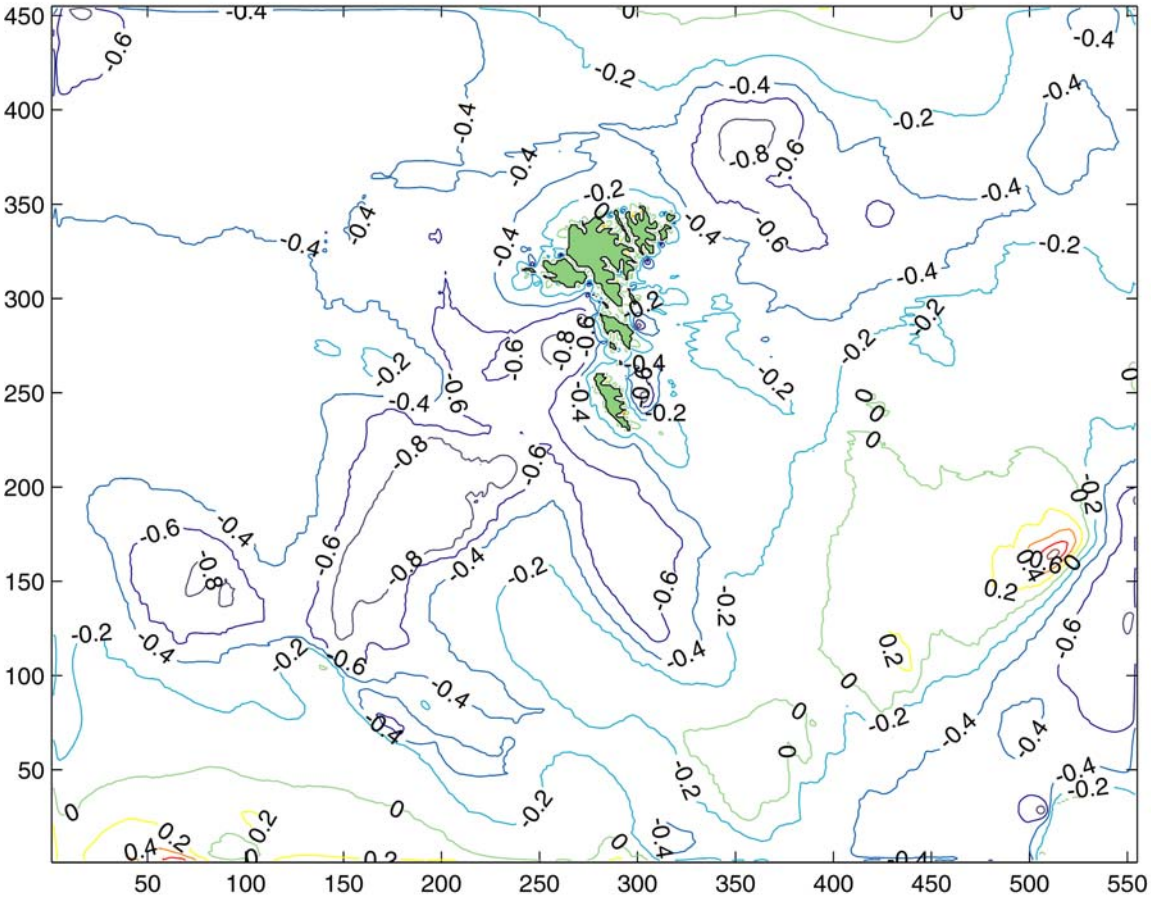

Figure 8.1. Polarisation of the M2 tidal ellipse ($P = U_{min}/U_{maj}$) calculated from the tidal simulation (Simonsen, 1999). Negative polarisation implies anti-cyclonic rotation.

9 Summary and concluding remarks

The data used to locate the Faroe Shelf Front and investigate cross frontal temperature differences are SST data measured at the bottom of R/V Magnus Heinason. These data are calibrated against CTD data and are found to have a typical standard error less than 0.05 °C.

It is found, that the temperature difference across the front is most pronounced in the spring, and that this can be explained by a simple heat budget – the on-shelf water is more effectively cooled during winter than the off-shelf water, creating a large temperature difference between the water masses in the early spring. A simple model is used to calculate the heat balance of the shelf and its surroundings. The temperature diffusion from off-shelf to on-shelf is calculated in discrete spatial steps but, nonetheless, the model reproduces the seasonal temperature variation fairly well, especially on-shelf.

The position of the front vs. bottom depth is discussed in relation to several theories. The H/U^3 theory can not predict the location of the front, and this is in agreement with the observations, which show that no seasonal variation is found in the location of the front. The simple bottom Ekman layer theory (Eq. 3.9) does not fit the observations, but it is found, that the theory by Soulsby (1983) fits the observed position of the front in most areas, as long as the surface mixed layer is ignored. The frontal bottom depth is found to be larger west of the islands than north and east of the islands. The reason for this is believed to arise from larger anticyclonic polarisation of the tidal ellipse and from frequent winds from the south west.

The collection of SST data from R/V Magnus Heinason continues and, of course, the statistics can be improved by including more tracks. Also, it is possible to acquire satellite-derived SST data of the Faroe Shelf Front, but presumably they require at least as much effort in quality control and analysis as do the R/V Magnus Heinason SST data. A thorough investigation of the front will also require CTD and preferably also ADCP transects across the front.

10 References

1. Allen, J. S., Beardsley, R. C., Blanton, J. O., Boicourt, W. C., Butman, B., Coachman, L. K., Huyer, A., Kinder, T. H., Royer, T. C., Schumacher, J. D., Smith, R. L., Sturges, W., and Winant, C. D. 1983. Physical Oceanography of Continental Shelves. Reviews of Geophysical and Space Physics, 21: 1149-1181.

2. Bertelsen, E. 1951. Occurrence of 0-group Cod, Haddock and Coalfish, Summer 1950. Annales Biologiques, 7: 27-28.

3. Cappelen, J and Laursen, E. V. 1998. The Climate of the Faroe Islands - with Climatological Standard Normals, 1961-1990. Danish Meteorological Institute Technical Report 98-14. 62 pp.

4. Chapman, D. C. 1986. A Simple Model of the Formation and Maintenance of the Shelf/slope Front in the Middle Atlantic Bight. Journal of Physical Oceanography, 16: 1273-1279.

5. Chapman, D. C. 2000. Boundary Layer Control of Buoyant Coastal Currents and the Establishment of a Shelfbreak Front. Journal of Physical Oceanography, 30 (11): 2941-2955.

6. Cushman-Roisin, B. 1994. Introduction to Geophysical Fluid Dynamics. Prentice-Hall, Inc., New Jersey, 320 pp.

7. Drinkwater, K. F. and Loder, J. W. 2001. Near-surface horizontal convergence and dispersion near the tidal-mixing front on Northeastern Georges Bank. Deep-Sea Research II 48: 311-339.

8. Ellet, D. J. and Debrah, J. K. 1974. Hydrographic observations at Faroe, 30 June - 12 July 1972. Annales Biologiques 29: 15-16.

9. Fearnhead, P. G. 1975. On the formation of fronts by tidal mixing around the British Isles. Deep-Sea Research, 22: 311-321.

10. Fraser, J. H. 1949. Plankton of the Faroe-Shetland Channel and the Faroes, June and August 1947. Annales Biologiques, 4: 27-28.

11. Gaard, E., Hansen, B., and Heinesen, S. 1998. Phytoplankton variability on the Faroe Shelf. ICES Journal of Marine Science, 55: 688-696.

12. Gaard, E. and Hansen, B. 2000. Variations in the advection of *Calanus finmarchicus* onto the Faroe Shelf. ICES Journal of Marine Science, 57: 1612-1618.

13. Gaard, E., Hansen, B., Olsen, B., and Reinert, J. 2002. Ecological Features and Recent Trends in the Physical Environment, Plankton, Fish Stocks, and Seabirds in the Faroe Shelf Ecosystem. *In* Large Marine Ecosystems of the North Atlantic, Changing States and Sustainability. *Edited by* K. Sherman and H. R. Skjoldal. Elsevier Science, Amsterdam, 245-265.

14. Hansen, B. 1979. Residual flow and temperature on the Faroe Plateau during the first half of 1978 in relation to the circulation. ICES CM 1979/C:18, 17 pp.

15. Hansen, B. 1992. Residual and tidal currents on the Faroe Plateau. ICES CM 1992/C:12, 18 pp.

16. Hansen, B., Stefansson, U., and Svendsen, E. 1998. Iceland, Faroe and Norwegian coasts. *In* The Sea, Vol 11, The Global Coastal Ocean, Regional Studies and Syntheses. *Edited by* A. R. Robinson and K. H. Brink. John Wiley & Sons, Inc., New York, 733-757.

17. Hansen, B. and Larsen, K. M. H. 1999. Traditional Current Meter Observations in Faroese Offshore Waters. The Faroese Fisheries Laboratory, Technical Report No. 99-01, 193 pp.

18. Hansen, B. 2000. Havið. Føroya Skúlabókagrunnur, Torshavn, 232 pp. (In Faroese)

19. Hansen, B. and Østerhus, S. 2000. North Atlantic-Nordic Seas exchanges. Progress in Oceanography, 45: 109-208.

20. Hansen, B., Østerhus, S., Hátún, H., Kristiansen, R., and Larsen, K. M. H. 2003. The Iceland-Faroe inflow of Atlantic water to the Nordic Seas. *Submitted to* Progress in Oceanography.

21. Knudsen, M. 1905. Contribution to the hydrography of the North Atlantic Ocean. Meddelelser fra Kommissionen for Havundersøgelser, Serie Hydrografi, I (6), 34 pp.

22. Knudsen, M. 1911. Danish hydrographical investigations at the Faroe Islands in the spring of 1910. Meddelelser fra Kommissionen for Havundersøgelser, Serie Hydrografi, II (1), 21 pp.

23. Larsen, K. M. H. 1999. Current Meter Observations in Faroese Inshore Waters 1979 - 1998. The Faroese Fisheries Laboratory, Technical Report No. 99-03, 172 pp.

24. Larsen, K. M. H., Hansen, B., Kristiansen, K., and Østerhus, S. 2000. Internal tides in the waters surrounding the Faroe Plateau. ICES CM 2000/L:09, 13 pp.

25. Larsen, K. M. H., Hansen, B., and Smith, L. 2001. The Front on the Faroe Shelf based on data logged by R/V Magnus Heinason 1999 - 2000. The Faroese Fisheries Laboratory, Technical Report No. 01-03, 13 pp.

26. Larsen, K. M. H., Hansen, B., Svendsen, H., and Simonsen, K. 2002. The front on the Faroe Shelf. ICES CM 2002/P:10, 15 pp.

27. Lindau, R. 2001. Climate Atlas of the Atlantic Ocean. Springer-Verlag, Berlin, 514 pp.

28. Loder, J. W., Wright, D. G., Garrett, C., and Juszko, B.-A. 1982. Horizontal Exchange on Central Georges Bank. Canadian Journal of Fisheries and Aquatic Sciences, 39: 1130-1137.

29. Loder, J. W. and Greenberg, D. A. 1986. Predicted positions of tidal fronts in the Gulf of Maine region. Continental Shelf Research, 6 (3): 397-414.

30. Mann, K. H. and Lazier, J. R. N. 1996. Dynamics of Marine Ecosystems. Blackwell Science, Inc., Malden, 394 pp.

31. Mavor, T. P. and Bisagni, J. J. 2001. Seasonal variability of sea-surface temperature fronts on Georges Bank. Deep-Sea Research II, 48: 215-243.

32. Pond, S. and Pickard, G. L. 1986. Introductory Dynamical Oceanography. Pergamon Press, Oxford, 329 pp.

33. Simonsen, K. 1999. Tides and tidal simulation in the area around the Faroe Islands. Nansen Environmental and Remote Sensing Center, Technical Report No. 166, 104 pp.

34. Simpson, J. H. and Hunter, J. R. 1974. Fronts in the Irish Sea. Nature, 250: 404-406.

35. Simpson, J. H. and Bowers, D. 1981. Models of stratification and frontal movement in shelf seas. Deep-Sea Research, 28A: 727-738.

36. Simpson, J. H. 1998. Tidal Processes in Shelf Seas. *In* The Sea, Vol 10, The Global Coastal Ocean, Processes and Methods. *Edited by* K. H. Brink and A. R. Robinson. John Wiley & Sons, Inc., New York, 113-150 pp.

37. Smed, J. 1953. Monthly Anomalies of the Surface Temperature in Areas of the northern North Atlantic in 1952. Annales Biologiques **9**: 16-19.

38. Soulsby, R. L. 1983. The Bottom Boundary Layer of Shelf Seas. *In* Physical Oceanography of Coastal and Shelf Seas. *Edited by* B. Johns. Elsevier Science, Amsterdam, 189-266.

39. Stigebrandt, A. 1988. A note on the locus of a shelf front. Tellus, 40A: 439-442.

Appendix A

Table A.1. List of all tracks included in the report. “Cruise” is the R/V Magnus Heinason cruise number, where the first 2 digits indicate the year. “No.” is a tally for observed front-track on the cruise. “Day” and “Month” are date of track. “DIR” is direction of track (see Chapter 4.4). “Track Straight” is an indication of how straight the track is. “Depth Monot.” is an indication of whether the depth varies monotonically along the track. The column “Temperature” has 5 sub-columns describing the temperature: “Cont. inc.” indicates whether the temperature is continuously increasing with depth; “Steep inc.” indicates whether there is a steep temperature increase with depth. A number in the cell is depth in meters where the steep increase occurs; “Incl. LM” and “Incl. SM” indicates if there are large meanders or small meanders respectively on the temperature vs. depth plot; “Max. diff.” is maximum temperature difference across the front – it is negative if the on shelf water is warmer than the off shelf water. “Group” indicates quality classification (see Chapter 4.4). The remaining columns are all describing the exponential fit, where “Fitting” tells whether the exponential fit is done automatically or manually. For description of the last 6 columns see Chapter 4.3.

					Track	Depth	Temperature											D1	D2
Cruise	No.	Day	Month	DIR	Straight	Monot.	Cont. inc.	Steep inc.	Incl. LM	Incl. SM	Max. diff.	Group	Fitting	A	B	C	D0	75%	75%
0008	4	1	3	E	+	(-)	(-)	-	-	+	0,92	II	manual	6,00	0,50	0,030	110	63	156
0032	2	11	5	E	(+)	+	+	-	-	+	1,65	I	automatic	6,97	0,84	0,035	116	76	155
0032	3	13	5	E	+	-	(-)	-	-	(+)	1,77	II	automatic	6,97	0,82	0,054	91	65	116
9908	1	21	2	E	-	(-)	(-)	-	-	-	0,65	III	manual	6,30	0,40	0,050	66		
9912	5	1	3	E	+	(+)	(+)	-	-	+	0,82	II	manual	5,95	0,45	0,030	95	48	141
9912	6	3	3	E	+	-	(-)	-	-	(+)	0,85	II	manual	5,95	0,41	0,040	110	75	144
9912	7	3	3	E	+	(+)	+	+ 80/90	-	+	1,18	I	automatic	5,78	0,55	0,099	84	69	98
9928	6	27	4	E	-	(-)	(+)	+ 100	-	(+)	1,11	IV							
9932	2	6	5	E	+	+	(+)	+ 90	-	-	1,05	IV							
9936	2	2	6	E	+	(+)	(+)	-	-	(+)	0,85	II	automatic	7,83	0,36	0,050	124	96	151
9936	4	9	6	E	+	(+)	+	-	-	(+)	0,63	III	manual	7,70	0,40	0,015	100		
9940	1	11	6	E	+	(-)	(-)	-	-	+	0,90	IV							
9944	2	22	6	E	(+)	(-)	-	-	-	+	0,62	IV							
9944	3	22	6	E	(-)	-	(+)	-	-	+	0,45	III	manual	8,55	0,25	0,050	140		
9948	3	5	7	E	+	(+)	+	-	-	-	1,14	II	manual	8,78	0,65	0,030	95	48	141
9952	2	6	8	E	+	+	+	-	-	(+)	1,71	II	manual	9,80	1,00	0,025	125	69	180
9956	2	15	8	E	-	(-)	-	-	+	-	0,99	IV							
9976	1	25	9	E	+	(+)	(+)	-	-	-	0,25	II	manual	10,11	0,12	0,200	113	106	119
0012	1	9	3	SE	(-)	(-)	(+)	-	-	-	0,85	III	automatic	5,91	0,40	0,042	106		
0026	1	19	4	SE	+	(+)	(+)	+ 80	-	-	0,47	I	automatic	5,87	0,25	0,120	77	65	88

Table A.1. Continued.

					Track	Depth	Temperature											D1	D2
Cruise	No.	Day	Month	DIR	Straight	Monot.	Cont. inc.	Steep inc.	Incl. LM	Incl. SM	Max. diff.	Group	Fitting	A	B	C	D0	75%	75%
0026	2	24	4	SE	+	(+)	(+)	(+ 80)	-	+	0,69	I	automatic	5,90	0,40	0,029	81	33	128
9912	1	27	2	SE	+	+	+	(+ 60)	-	-	0,89	II	manual	5,90	0,48	0,050	90	62	117
9912	2	27	2	SE	(+)	(+)	(+)	-	-	-	0,27	III	manual	6,60	0,14	0,060	85		
9936	3	2	6	SE	+	+	-	-	+	-	0,32	IV							
9950	1	30	7	SE	+	+	(+)	+ 80/90	-	-	0,90	I	automatic	9,69	0,43	0,120	86	74	97
9952	1	6	8	SE	(+)	(+)	(+)	+ 80	-	-	1,07	I	automatic	9,72	0,48	0,097	79	64	93
9956	1	13	8	SE	+	+	+	-	-	-	0,76	I	automatic	9,89	0,33	0,083	93	76	109
0028	1	29	4	N	+	+	(-)	-	-	+	0,80	III	manual	6,00	0,43	0,120	124		
0032	4	25	5	N	(+)	+	(+)	-	-	(+)	1,37	I	automatic	6,93	0,69	0,045	116	85	146
0032	5	25	5	N	-	+	(+)	-	-	(+)	1,28	III	manual	7,10	0,60	0,050	90		
9908	2	24	2	N	+	+	(-)	(+ 90)	-	+	1,44	IV							
9916	1	12	3	N	+	+	(-)	-	-	+	1,37	II	manual	5,70	0,78	0,025	112	56	167
9932	3	6	5	N	(+)	+	-	(+)	+	-	0,83	IV							
9932	4	25	5	N	(+)	+	(-)	-	-	+	1,18	II	manual	7,40	0,70	0,030	125	78	171
9940	3	13	6	N	(+)	+	(+)	+ 80	-	+	1,35	I	automatic	8,06	0,55	0,100	92	78	105
9940	4	14	6	N	(+)	+	+	-	-	(+)	1,16	I	automatic	8,02	0,50	0,074	116	97	134
9948	1	3	7	N	+	+	+	-	-	-	1,27	II	manual	8,68	0,68	0,035	135	95	174
9964	1	10	9	N	(+)	+	-	-	-	-	-0,06	IV							
9988	2	9	11	N	(+)	(+)	-	-	-	+	-0,48	IV							
0008	1	25	2	S	(+)	-	-	-	-	+	0,84	IV							
0008	2	25	2	S	+	(+)	(-)	-	-	+	0,35	II	manual	6,67	0,18	0,070	160	140	179
0016	1	17	3	S	+	(+)	(-)	-	-	+	0,63	IV							
0016	4	18	3	S	(+)	-	-	(+ 60)	+	-	0,45	II	manual	6,25	0,11	0,200	112	105	118
9992	1	12	11	S	+	-	-	-	-	+	0,15	IV							
0028	2	30	4	NW	(+)	(+)	(+)	+ 100/110	-	(+)	1,69	II	manual	6,25	0,84	0,150	102	92	111
0032	6	28	5	NW	(+)	(+)	(+)	-	-	-	1,66	III	manual	6,98	0,68	0,056	119		
9916	2	16	3	NW	-	(+)	(-)	+ 95	(+)	-	1,16	III	manual	6,20	0,60	0,200	98		
9916	3	16	3	NW	(+)	(+)	+	+ 100	-	-	1,31	I	automatic	5,71	0,63	0,120	101	89	112
9928	3	25	4	NW	-	(+)	(+)	+ 110	-	(+)	1,62	III	automatic	6,26	0,87	0,120	110		
9928	4	25	4	NW	-	(+)	-	+ 95	-	+	1,41	III	manual	6,50	0,50	0,200	96		
9928	5	26	4	NW	+	(+)	-	+ 100	+	-	1,18	IV							
9944	1	20	6	NW	-	-	-	+ 110	+	+	0,94	IV							

Table A.1. Continued.

					Track	Depth	Temperature											D1	D2
Cruise	No.	Day	Month	DIR	Straight	Monot.	Cont. inc.	Steep inc.	Incl. LM	Incl. SM	Max. diff.	Group	Fitting	A	B	C	D0	75%	75%
0008	3	26	2	SW	+	(+)	-	+ 90	-	+	0,93	IV							
0016	6	22	3	SW	(+)	+	-	+ 150	-	+	0,84	IV							
0020	1	30	3	SW	+	(+)	(+)	-	-	-	1,14	II	automatic	6,37	0,53	0,065	135	113	156
0020	2	4	4	SW	+	+	+	-	-	(+)	0,83	II	manual	5,90	0,50	0,020	145	75	214
0024	2	17	4	SW	+	+	(+)	(+ 150)	-	-	1,33	II	manual	5,95	0,73	0,030	140	93	186
0032	1	6	5	SW	(+)	(+)	-	+ 80/110	+	-	1,27	IV							
0068	1	15	9	SW	+	+	-	+	+	-	1,11	IV							
9912	4	1	3	SW	(+)	+	+	-	-	-	0,75	I	automatic	6,05	0,36	0,037	114	76	151
9916	4	26	3	SW	+	+	+	-	-	-	1,16	I	automatic	5,94	0,55	0,048	111	82	139
9924	2	20	4	SW	+	+	-	-	-	-	0,61	III	manual	6,35	0,30	0,060	145		
9932	1	1	5	SW	+	+	(+)	+ 170	-	-	0,92	II	manual	6,80	0,37	0,150	164	154	173
9940	2	13	6	SW	+	+	+	+ 160	-	-	1,10	I	automatic	8,48	0,51	0,120	156	144	167
9944	4	26	6	SW	-	(+)	+	-	-	-	0,65	III	automatic	8,51	0,30	0,056	131		
9944	5	29	6	SW	+	+	-	+ 150	-	+	1,33	IV							
9960	1	29	8	SW	+	+	(-)	-	(+)	-	0,85	IV							
9964	2	14	9	SW	(+)	+	-	(+ 160)	(+)	-	0,51	IV							
9972	1	17	9	SW	+	+	(-)	+ 170	-	(+)	0,76	II	manual	9,76	0,40	0,300	168	163	172
9984	2	29	10	SW	+	+	-	-	-	-	-0,11	IV							
9984	3	29	10	SW	+	+	-	-	-	-	-0,07	IV							
0016	2	17	3	SSW	(+)	-	(-)	(+ 150)	-	+	0,79	III	manual	6,26	0,35	0,200	150		
0016	3	18	3	SSW	(-)	-	(-)	(+ 140)	-	+	1,12	III	manual	6,24	0,50	0,200	140		
0024	1	6	4	SSW	+	(+)	+	-	-	-	2,16	II	manual	6,20	1,20	0,040	170	135	204
0036	1	1	6	SSW	+	(+)	-	+ 180	-	-	1,69	II	manual	7,45	0,85	0,150	182	172	191
9912	3	28	2	SSW	(+)	+	(-)	+ 170	-	+	1,61	II	manual	6,35	0,76	0,100	173	159	186
9924	1	10	4	SSW	+	-	(-)	-	-	(+)	1,49	IV							
9928	1	23	4	SSW	(+)	(+)	+	-	-	+	0,96	IV							
9936	1	28	5	SSW	+	(+)	(-)	+ 160	-	+	1,19	II	manual	7,50	0,56	0,120	162	150	173
9950	2	3	8	SSW	+	-	-	-	+	+	1,51	IV							
9984	1	22	10	SSW	+	(+)	-	(+ 180)	(+)	-	0,29	IV							
9992	2	15	11	SSW	+	-	-	-	-	+	-0,22	IV							
0004	1	11	2	W	+	(+)	-	+ 140	-	+	0,86	II	manual	6,95	0,41	0,150	145	135	154
0028	3	1	5	W	-	-	-	+ 110	+	-	1,93	IV							

Table A.1. Continued.

					Track	Depth	Temperature											D1	D2
Cruise	No.	Day	Month	DIR	Straight	Monot.	Cont. inc.	Steep inc.	Incl. LM	Incl. SM	Max. diff.	Group	Fitting	A	B	C	D0	75%	75%
0072	1	3	10	W	+	+	+	+ 150	-	-	0,56	I	automatic	10,06	0,27	0,100	148	134	161
0084	1	2	11	W	+	(+)	-	-	-	+	0,20	IV							
9912	8	9	3	W	+	+	(+)	-	-	+	1,63	II	manual	5,80	0,90	0,030	150	103	196
9928	2	24	4	W	(+)	(+)	-	+ 180	-	+	1,46	III	manual	6,80	0,60	0,300	184		
9948	2	3	7	W	+	(+)	-	-	-	+	1,43	IV							
9960	2	30	8	W	-	-	-	-	+	-	1,04	IV							
9976	2	6	10	W	+	(+)	-	-	-	+	0,28	IV							
9988	1	5	11	W	+	(+)	(+)	-	-	(+)	0,21	II	automatic	9,18	0,11	0,043	136	103	168

Appendix B Data from a tidal simulation

To test the observed frontal location against the theories on tidal fronts described in Chapter 3, data from a tidal model are used. First a description of the model used in this thesis is given, followed by a description of which data are extracted from the model and how tidal velocities are averaged and cubed.

Description of the model

The tidal model used in this thesis is from Simonsen (1999). The model describes the entire Faroe Plateau and the surroundings to the south and west. It has a grid size of 0.5x0.5 nautical miles and has 455 x 555 grid points. It is a barotropic model, meaning that it only has one layer, and that the current is assumed to be the same through the whole water column. This is fairly realistic for the on-shelf water, but not for off-shelf waters (Larsen *et al.*, 2000). Figure B.1 shows the model domain with bathymetry.

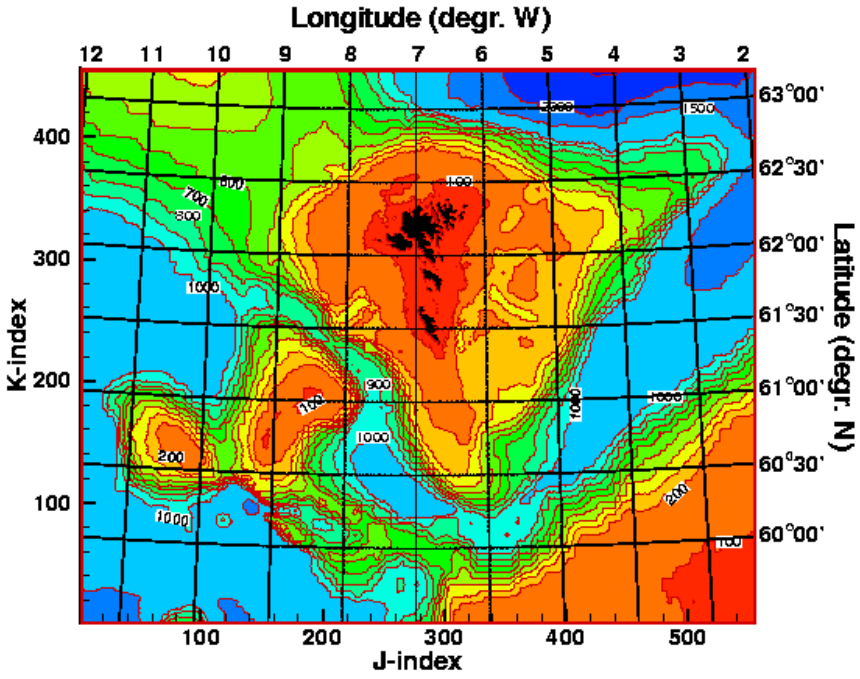

Figure B.1. Model domain and bathymetry.

The output from the model is both elevation and current data and includes eight constituents: K_1, K_2, M_2, N_2, O_1, P_1, Q_1 and S_2. The current data are represented with the tidal ellipse parameters. In calculating the tidal current, only the parameters major and minor semi axes are used, since only the length of the velocity vector is needed

and not the direction. It can be noted, that the M_2 semi axes are somewhat underestimated as a whole in the model.

Extraction of data

The data used to test the frontal theories are the depth matrix H and the M_2 major and minor semi-axes matrices. To calculate the mean M_2 speed (U) and M_2 speed cubed (U^3), the M_2 major (A) and minor (B) semi-axes matrices are used, where each number in the matrix represents a grid point. Time averaged over a tidal period (T), the M_2 speed becomes:

$$U = \left(\frac{1}{T} \int_0^T \left(A^2 \cos^2(\omega t) + B^2 \sin^2(\omega t) \right) dt \right)^{1/2} = \left(\frac{1}{2} \left(A^2 + B^2 \right) \right)^{1/2} \text{ where } \omega = \frac{2\pi}{T} \quad \text{(B.1)}$$

Similarly the M_2 speed cubed becomes

$$U^3 = \frac{1}{T} \int_0^T \left(A^2 \cos^2(\omega t) + B^2 \sin^2(\omega t) \right)^{3/2} dt \quad \text{(B.2)}$$

and, since this integration is not easily solved, the integration is done in a Matlab routine. These velocities are then used to calculate H/U^3 and H/U, where H is the topography matrix from the model.